Alexei Kuzmin

EDA:
EXAFS Data Analysis
Software Package

User's Manual

Version 9.0

Riga 2016

Copyright

Warranty

System Requirements

To use the EDA package, you must have IBM PC compatible computer[1] running MS Windows XP/Vista/7/8/10[2] operating system.

---

[1] IBM are the trade-marks of International Business Machines Corporation.
[2] Microsoft, MS, MS-DOS, Windows are the trade-marks of Microsoft Corporation

Preface

X-ray absorption spectroscopy (XAS) is a powerful tool to study *local* electronic and atomic structure of solids, liquids and gases in a wide range of external conditions defined by temperature, pressure, etc. The information can be extracted from the extended X-ray absorption fine structure (EXAFS) having the oscillating character and located beyond the absorption edge of an atom. The EXAFS range extends for about 400–1000 eV above the edge due to limitations caused by experimental noise and/or by the presence of another absorption edge. General approach to the analysis of EXAFS spectra has been developed during last decades [1]. It requires an intensive use of modern computers, which allow one to carry out real-time interactive data analysis.

In the present guide, the conventional approach to the EXAFS data analysis is described based on the author's 20 years experience in the field. It is implemented in the EDA software package [2], which is available for download at
<div align="center">

`http://www.dragon.lv/eda/`.

</div>

An attempt to implement the existing theory in a set of programs for IBM PC compatible computers has been started by the author in 1988 at the Institute of Solid State Physics (Riga, Latvia). As a result of the project, the **E**XAFS **D**ata **A**nalysis software package, called EDA, has appeared. It has been tested on a number of applications [2, 3] and showed good results and flexibility in the analysis of experimental data. The EDA package is generally based on the conventional EXAFS analysis procedure, however, some original tricks and approaches are included.

The author wish to thank Dr.hab. J. Purans for the continuous support and interest in the development of the EDA package.

Please cite the following article if results, obtained by the EDA code are used in published work:
<div align="center">

A. Kuzmin, Physica B 208/209 (1995) 175-176.

</div>

Riga, June, 2015.   ALEXEI KUZMIN

Contents

Abbreviations

BFT	Back Fourier Transform
EDA	**EXAFS Data Analysis** software package
EXAFS	Extended X-ray Absorption Fine Structure
FMS	Full Multiple-Scattering
FT	Fourier Transform
MC	Monte Carlo
MD	Molecular Dynamics
MFP	Mean Free Path
MS	Multiple-Scattering
RDF	Radial Distribution Function
RMC	Reverse Monte Carlo
XANES	X-ray Absorption Near Edge Structure
XAFS	X-ray Absorption Fine Structure
XAS	X-ray Absorption Spectroscopy

Chapter 1

Introduction

1.1 The EDA package

The EDA package allows one to perform all steps of the EXAFS data analysis and consists of the nine programs (see Table 1.1). The code was developed with the idea to be intuitively simple and fast, guiding the user step by step through each part of the analysis. The code has been intensively used and tested on a number of applications [2, 3] and showed good results and flexibility in the analysis of experimental data.

There are three main differences from known packages. First, an improved algorithm is used for atomic-like background removal in the EXAFS extraction procedure. Second, a non-linear least-squares fitting program for EXAFS, based on a high speed algorithm without matrix inversion (instead of usual Marquardt method), was developed and allows simultaneous analysis up to 20 shells with 8 fitting parameters ($S_0^2 N_i$, R_i, σ_i^2, ΔE_{0i}, C_{3i}, C_{4i}, C_{5i} and C_{6i}) in each. The range of values of any fitting parameter can be limited by boundaries or fixed to a constant value. The covariance and correlation matrices can be also calculated. Third, a possibility for the *model independent* derivation of the radial distribution function (RDF) from the EXAFS spectrum using the general model (Fig. 1.1) is available.

Next we will briefly introduce the reader into the conventional EXAFS analysis methodology and discuss shortly its main concepts (Fig. 1.1). The technical details of each analysis step are given in the following sections.

One normally starts with the experimental data, for example, by measuring x-ray intensities before $I_0(E)$ and after $I(E)$ the sample using two ionization chambers in the transmission mode. These two quantities are used next to calculate the x-ray absorption coefficient, defined as $\mu(E) = \ln(I_0(E)/I(E))$, by the EDAFORM code (or any other suitable codes).

Thus obtained x-ray absorption coefficient $\mu(E)$ can be separated into (i) the XANES

Table 1.1: A set of programs for EXAFS data analysis and simulations included in the EDA software package.

Code title	Code description
EDAFORM	converts original experimental data from several beamlines into the EDA file format (ASCII, 2 columns).
EDAXANES	extracts the XANES part of the experimental X-ray absorption spectrum and calculates its first and second derivatives.
EDAEES	extracts the EXAFS part $\chi(k)$ using original algorithm for the atomic-like ("zero-line") background removal.
EDAFT	performs Fourier filtering procedure (direct and back Fourier transforms) with or without amplitude/phase correction using a number of different (rectangular, Gaussian, Kaiser-Bessel, Hamming and Norton-Beer F3) window functions.
EDAFIT	is a non-linear least-squares fitting code, based on a high speed algorithm without matrix inversion. A multi-shell Gaussian or cumulant model within the single-scattering approximation can contain up to 20 shells with up to 8 fitting parameters (N_i, S_o^2, R_i, σ_i^2, ΔE_{0i}, C_{3i}, C_{4i}, C_{5i}, C_{6i}) in each. Constrains on the range of any fitting parameter or its value can be imposed.
EDARDF	is the regularization-like least-squares-fitting code allowing one to determine model-independent RDF in the first coordination shell for a compound with arbitrary degree of disorder.
FTEST	performs analysis of variance of the fitting results based on the Fisher's $F_{0.95}$-test.
EDAPLOT	is a general-purpose program for plotting, comparison, and mathematical calculations frequently used in the EXAFS data analysis (more than 20 different operations).
EDAFEFF	extracts the scattering amplitude and phase shift functions from FEFF****.dat files, calculated by the FEFF8/9 code, for the use with the EDAFIT or EDARDF codes.
EDACA	calculates configuration-averaged EXAFS based on the results of molecular dynamics simulations.

part, located close to the x-ray absorption edge, by the EDAXANES code and (ii) the total experimental EXAFS signal $\chi(k)$ by the EDAEES code.

After total experimental EXAFS signal $\chi(k)$ extraction, one usually performs its Fourier filtering (i.e. direct and back Fourier transforms (FT) with some suitable "window"-function) to separate contribution from different structural shells (peaks in FT). This is done by the EDAFT code. Such approach allows one to "simplify" the analysis, at least, for the first coordination shell of the absorbing atom.

Finally, the EXAFS signal from a single shell can be simulated using different models to extract structural information. The EDA package allows one to use three models: (i) conventional multi-component parameterized model within the Gaussian or cumulant approximation (the EDAFIT code), (ii) arbitrary radial-distribution function (RDF) model obtained by the regularization-like approach(the EDARDF code), (iii) the so-called
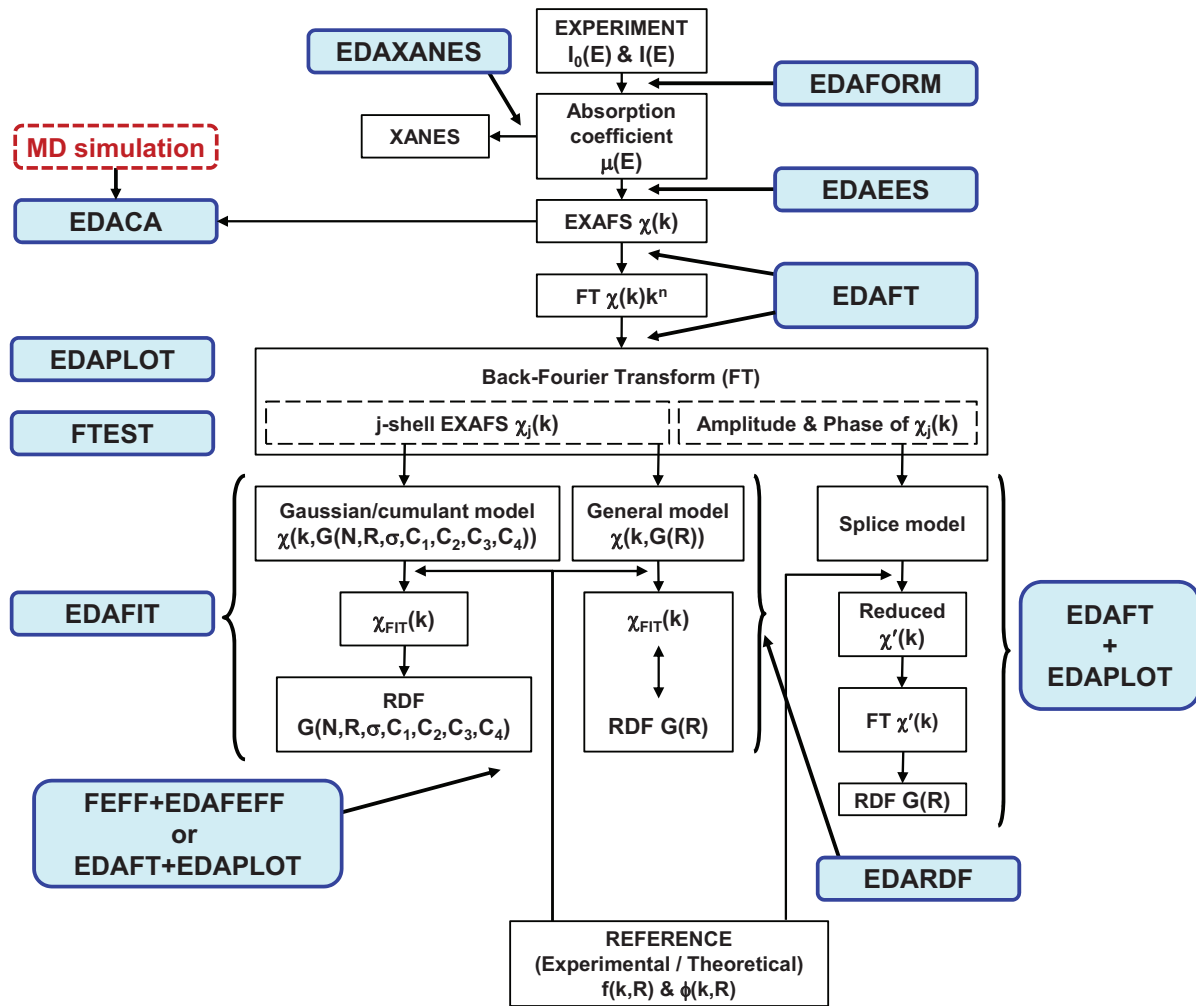
Figure 1.1: Flowchart of the EXAFS data analysis by the EDA package.

"splice" model (one need to use the EDAFT and EDAPLOT codes). To perform simulations, one obviously needs to provide the scattering amplitude and phase shift functions for each scattering path. These data can be obtained either from experimental EXAFS signal for etalon (reference) compound or calculated theoretically. In the EDA package, one has possibility to use the theoretical data calculated by the FEFF code [4], which can be extracted from the feff****.dat files by the EDAFEFF code.

Different models obtained from the simulations of the EXAFS signal by the EDAFIT code can be compared to the experimental EXAFS signal by the FTEST code, applying the Fisher's $F_{0.95}$ criterion.

Finally, visualization, comparison and simple mathematical analysis of any obtained data can be done using the EDAPLOT code. Note that since all data are kept in the simple ASCII format, they can be easily transferred to and treated by any other codes.
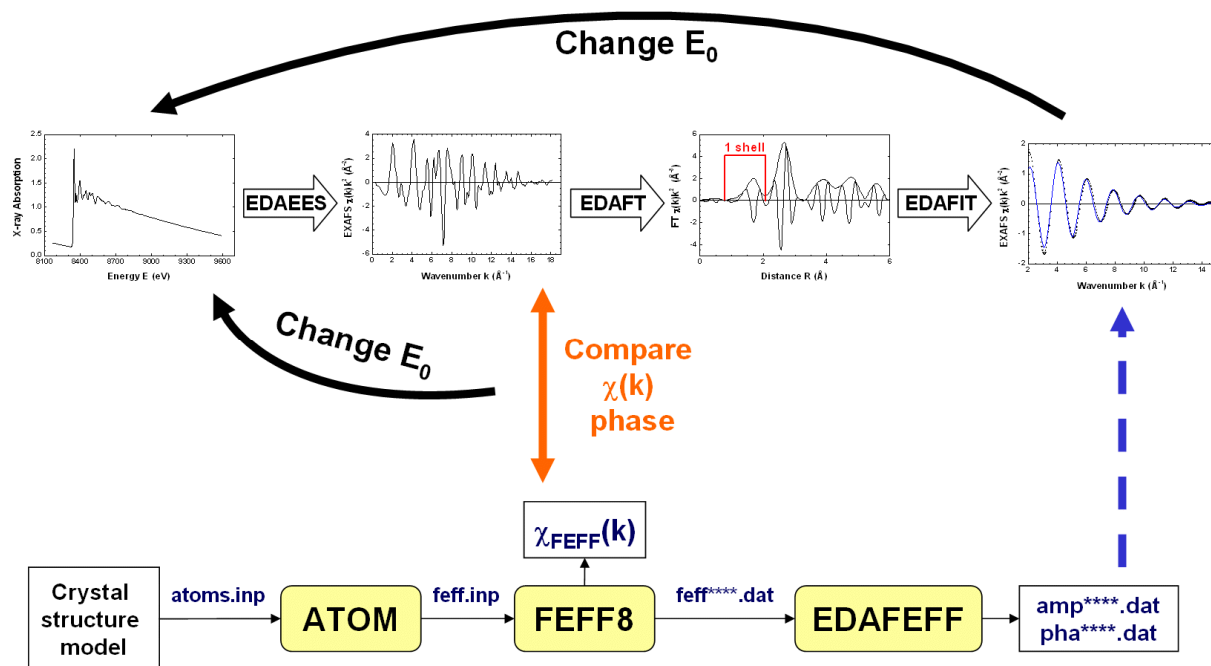
Figure 1.2: General methodology of the first shell EXAFS analysis.

1.2 EXAFS analysis methodology

The methodology of the EXAFS data analysis using the EDA package and theoretical amplitude and phase shift functions, calculated by the FEFF code [4], is shown in Fig. 1.2.

It is crucial to align the experimental data and the theory on the same wavenumber scale (k-scale), since there is strong correlation between the origin of the photoelectron kinetic energy E_0 and the interatomic distances R (both parameters influence the frequency of the EXAFS signal). Therefore, one normally starts from the analysis of the EXAFS signal for the reference compound, whose atomic structure is well known. A good polycrystalline compound with the local structure close to that of the sample under study is a good choice for the reference.

As the first trial, one can set the position of E_0 at the maximum of the first derivative of the x-ray absorption coefficient and extract the EXAFS signal $\chi(k)$: this should be done by the EDAEES code. Besides, one needs to perform calculation of the theoretical total EXAFS signal $\chi_{\text{FEFF}}(k)$ by the FEFF code [4]. This requires the construction of the feff.inp file for the reference compound, which can be done by the ATOMS code.

After executing the FEFF code [4], the theoretical EXAFS signal should be extracted from the generated chi.dat file and compared with the experimental one. If the phases of two EXAFS signals deviate significantly, especially in the low-k range, one needs to adjust the E_0 position for the experimental EXAFS signal. Thus, the whole extraction procedure should be repeated till the two EXAFS signals will be aligned with the accuracy

of better than 0.5-1 eV. When the good position of E_0 for the EXAFS spectrum of the reference compound is found, the same E_0 value should be used for other EXAFS signals under analysis.

As a result of the FEFF calculation for the reference compound, a set of feff****.dat files is also generated for all scattering paths. Each feff****.dat file can be used to generate by the EDAFEFF code a pair of files (amp****.dat and pha****.dat) containing the amplitude and phase shift functions in the format required by the EDAFIT and EDARDF codes. Here the asterisk symbol should be changed by the required scattering path number, for example, amp0001.dat.

After proper selection of the E_0 value, one can continue the analysis of the EXAFS spectrum for the system of interest. In many cases, due to the presence of the multiple-scattering contributions at large distances, only analysis of the first coordination shell of the absorber can be rigorously performed, i.e. without further significant approximations.

To do this, one needs first to isolate the contribution of the first shell by performing direct and back Fourier transformations (FT) of the experimental EXAFS signal. This can be done by the EDAFT code. One should take care that exactly the same "windows"-function is used in k-space, and the "window"-function in R-space selects precisely the range of the first shell. The overlap with the outer shells in R-space, the noise and the presence of the phase shift must be taken into account to do the isolation procedure properly.

Finally, the isolated first shell EXAFS signal can be best-fitted by the Gaussian or cumulant model using the EDAFIT code, or the first shell RDF function can be directly reconstructed by the EDARDF code. In both cases, the amplitude (amp****.dat) and phase shift (pha****.dat) functions must be provided.

Chapter 2

Description of the EXAFS data analysis

The **EDA** software package consists of a set of interactive programs (**EDAFORM, EDAXANES, EDAEES, EDAFEFF, EDAFT, EDAFIT, EDARDF, FTEST, EDAPLOT** and **EDACA**), which allow one to carry out all steps of the EXAFS data analysis procedure and will be described below.

Few internal agreements exist within the **EDA** package:

- All files have *two columns* ASCII format: the *first* column contains the information about a function (e.g. the absorption coefficient, the EXAFS signal, the scattering amplitude or phase, etc.) and the *second* one is its argument (energy, wave vector or distance). The use of the ASCII format allows one to view and to modify the content of a file using any simple editor and to import a file into different drawing programs.

  There is an exception for the output file after Fourier transform (FT): it has four columns corresponding to the distance, the imaginary and real parts of FT, and the FT modulus.

- It is assumed that the names of files related to the spectral or structural functions (as the absorption coefficient, the EXAFS signal, the FT, the RDF, etc.) have the extension .**TXT** and to the scattering amplitude and phase functions the extension .**DAT**, however other extensions can be also used.

2.1   Convertion of experimental data into the EDA format

The EDAFORM program allows one to prepare the experimental data, measured at different EXAFS stations, for further use within the EDA software package. At present time, 19 formats of the experimental data are supported:

0. Arbitrary ASCII file

1. PWA absorption (ADONE, Frascati)

2. PWA fluorescence (ADONE, Frascati)

3. PULS absorption (ADONE, Frascati)

4. LURE absorption (DCI, Orsay)

5. LURE fluorescence (DCI, Orsay)

6. GILDA absorption (ESRF, Grenoble)

7. GILDA fluorescence (ESRF, Grenoble).

8. GILDA multi-detector fluorescence (ESRF, Grenoble).

9. BM29 absorption (ESRF, Grenoble).

10. BM29 multi-detector fluorescence (ESRF, Grenoble).

11. BM29 absorption with 2 samples (ESRF, Grenoble).

12. ID22 fluorescence (ESRF, Grenoble).

13. DESY X absorption (HASYLAB, Hamburg).

14. BM29 fluorescence (ESRF, Grenoble).

15. ANKA absorption (KIT, Karlsruhe).

16. ANKA fluorescence (KIT, Karlsruhe).

17. DESY C absorption (HASYLAB, Hamburg).

18. DESY C fluorescence (HASYLAB, Hamburg).

The output file has *two column* ASCII format: the first column corresponds to the absorption coefficient ($\mu_{\text{exp}}(E)$), and the second one to the energy (E) in eV. If one has experimental data taken at another EXAFS station, it is necessary to transfer them into above described format before the use within the EDA package.

2.2   Extraction of the x-ray absorption near edge structure (XANES)

The EDAXANES program allows one to single out the XANES part (μ_{XANES}) of x-ray absorption spectra and to calculate the first ($d\mu/dE$) and second ($d^2\mu/dE^2$) derivatives of the absorption coefficient ($\mu(E)$). It can be useful for qualitative analysis of the near edge structure and for the determination of the precise position of the absorption edge (see, section 2.3). An example of the normalized XANES signal and its first and second derivatives is shown in Fig. 2.1 for the Re L_3-edge in ReO_3.
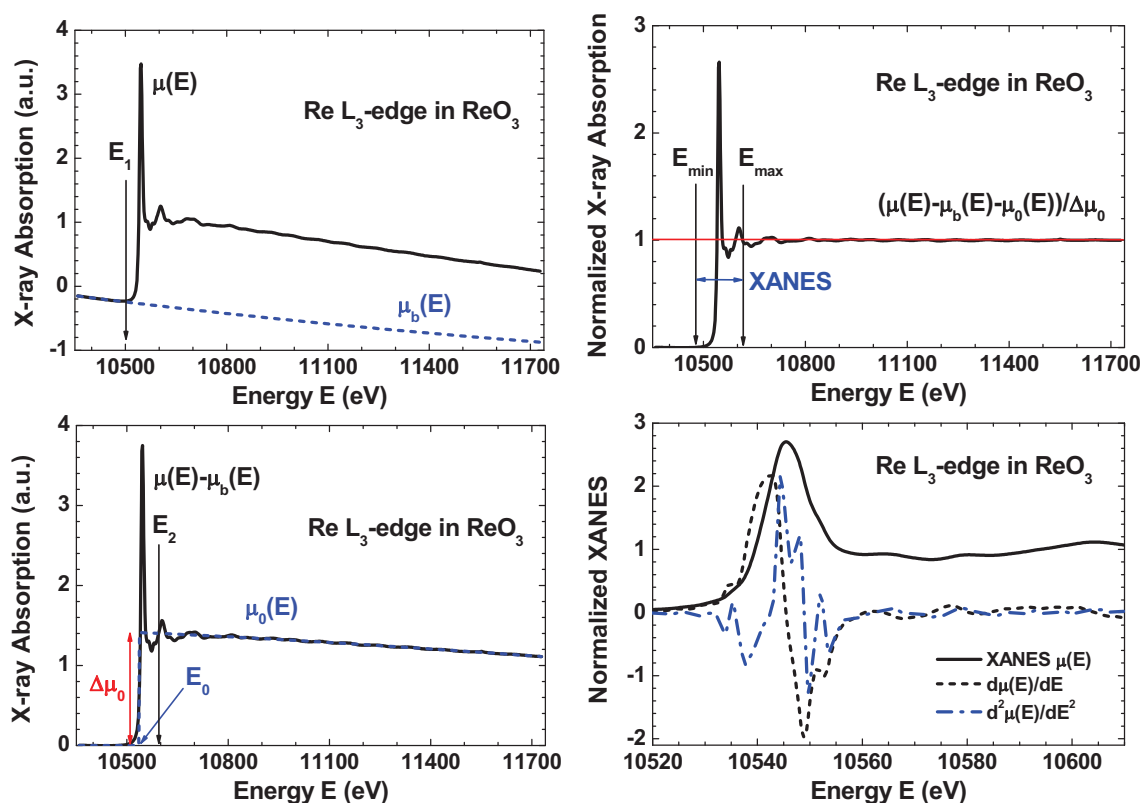
Figure 2.1: Extraction of the XANES part from the experimental x-ray absorption spectrum $\mu(E)$ at the Re L_3-edge for ReO_3. Normalized XANES ($\mu_{\text{XANES}}(E)$) (solid line) and its first $d\mu/dE$ (dashed line) and second $d^2\mu/dE^2$ (dash-dotted line) derivatives are shown in the right lower panel. See text for details.

The procedure to single out the XANES part is similar to that described in section 2.3. First, one needs to define the end of the background $\mu_b(E)$ before the edge by specifying E_1 energy point. Next, the E_0 energy should be set: the value of the absorption coefficient at this point will be used for normalization. Finally, the beginning of the atomic-like absorption $\mu_0(E)$ given by the E_2 energy should be set.

After, background subtraction and normalization, the required range from $E_{\min}$ to $E_{\max}$ of the XANES should be given and the number of energy points n specified. When this number n is larger than that in the experimental XANES, the interpolation is automatically performed by a cubic spline. Otherwise, original experimental points are used. The normalized XANES is defined as $\mu_{\mathrm{XANES}} = (\mu(E) - \mu_b(E) - \mu_0(E))/\Delta\mu_0$.

2.3 Extraction of the extended x-ray absorption near edge structure (EXAFS)

The EDAEES program allows one to extract the EXAFS signal $\chi(k)k^n$ from an x-ray absorption coefficient $\mu_{\exp}(E)$ given in the energy range from $E_{\min}$ to $E_{\max}$.

At the beginning, the background contribution $\mu_b(E)$ is approximated by the modified Victoreen polynomial ($\mu_b = A + B/E^3$) and subtracted from the experimental spectrum $\mu_{\exp}(E)$ (Fig. 2.2). The $\mu_b(E)$ function is calculated in the energy range from $E_{\min}$ to E_1 using the least-square procedure and extrapolated till $E_{\max}$.

Further, the atomic-like contribution $\mu_0(E)$ is found in a three-step procedure to have a precise removal of the EXAFS-signal zero-line. This point is very important since inaccuracies in $\mu_0(E)$ can lead after Fourier filtering procedure to a distortion of the first shell EXAFS signal and an additional noise in EXAFS from outer shells. Besides $\chi(k)$ signal is usually multiplied in the EXAFS analysis by a factor $k^n, n = 1, 2, 3$ (k is the photoelectron wave vector), therefore the requirements to the extraction of $\mu_0(E)$ become even higher, since the error introduced by $\mu_0(E)$ into EXAFS signal will be magnified several times. On practice, the three-step procedure is realized as follows.

At the first step, $\mu_0(E)$ is approximated by a polynomial $\mu_0'(E)$ (Fig. 2.2) of a power m_1 (the choice m_1=2 or 3 is recommended), which is than subtracted from $\mu = \mu_{\exp} - \mu_b$. The $\mu_0'(E)$ polynomial is calculated in the energy range from E_2 to E_3 (usually $E_3 = E_{\max}$) using the least-square procedure and extrapolated till $E_{\min}$.

The new function $\mu'(E) = \mu(E) - \mu_0'(E)$ (Fig. 2.3) is converted into the k-space and multiplied by a factor k^n with n equal or greater than the value, which one plans to use later in the analysis. The k is defined as $k = \sqrt{(2m/\hbar^2)(E - E_0)}$ where E_0 is usually related to to the Fermi level [4, 5].
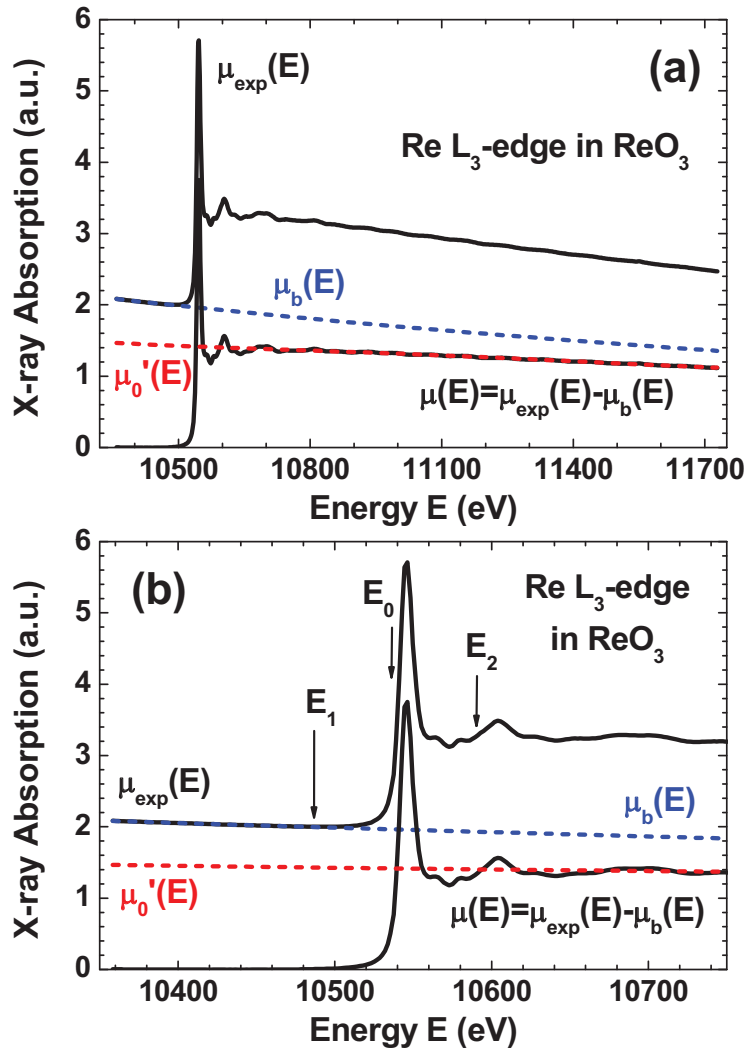
Figure 2.2: (a) The experimental x-ray absorption spectrum of the Re L_3-edge in ReO_3 before (μ_{exp}) and after (μ) subtraction of the background contribution μ_b. The first-step atomic-like contribution $\mu_0'(E)$ is also shown. (b) The enlarged region in the vicinity of the absorption edge. The position of three energies (E_1, E_0 and E_2), discussed in the text, are also shown.

At the second step, the zero-line function $\mu_0''(k)$ (Fig. 2.3) of $\mu'(k)$ is approximated by the polynomial of power m_2, which has the value between 0 and 9, and the function $\mu''(k) = \mu'(k) - \mu_0''(k)$ is calculated (Fig. 2.3). The need of the second step is that after conversion to the k space with simultaneous multiplication by the factor k^n, the function $\mu'(k)$ can have strongly distorted behaviour especially at high k values.

Thus, the idea of the first two steps is to obtain a function $\mu''(k)$ which is enough well but not obligatory perfectly oscillating around zero within all range of k.

At the third step, the *accurate* zero-line $\mu_0'''(k)$ (Fig. 2.3) of $\mu''(k)$ is finally obtained by the cubic-smoothing-spline technique. It is defined as $\mu_0'''(k) = \sum_i (a_i k^3 + b_i k^2 + c_i k + d_i)$

where i runs over all experimental points. The coefficients a_i, b_i, c_i and d_i satisfy to two criteria: (1) the function $\mu_0'''(k)$ and its first and second derivatives should be continuous, and (2) the sum of $[\mu_0'''(k)-\mu''(k)]^2$ over all points is equal to a number called the parameter of smoothing s (it should be provided by user). The value of s should be chosen in such way that the function $\mu_0'''(k)$ will allow one to eliminate from $\mu''(k)$ the low-frequency component without any distortion of the EXAFS oscillations, especially, that of the first shell. This can be controlled by comparing the Fourier transforms of the EXAFS signals with and without $\mu_0'''(k)$ contribution. The obtained $\mu_0'''(k)$ function is subtracted from $\mu''(k)$ giving the non-normalized EXAFS signal $\bar{\chi} = \mu - \mu_b - \mu_0$ where the function μ_0 is equal to the sum of μ_0', μ_0'' and μ_0'''.

The EXAFS-signal $\chi(E)$ is determined as $\chi = \bar{\chi}/\bar{\mu}_0 = (\mu - \mu_b - \mu_0)/\bar{\mu}_0$. Here $\bar{\mu}_0$ is equal to μ_0 of the analysed spectrum or can be substituted by the *properly normalized* reference function μ_0^{ref}: $\bar{\mu}_0 = \mu_0^{\text{ref}}(\Delta\mu_{\text{exp}}/\Delta\mu_{\text{ref}})$ where $\Delta\mu_{\text{exp}}$ and $\Delta\mu_{\text{ref}}$ are the edge jumps of the analysed and reference spectra, respectively. Here the quantities $\Delta\mu_{\text{exp}}$ and $\Delta\mu_{\text{ref}}$ are calculated from the μ' signals by averaging over the first five points therefore the correct behaviour of the μ' signals is essential to have correctly normalized EXAFS signals.

Finally, the obtained EXAFS-signal $\chi(E)$ is converted into k-space and can be multiplied by a factor k^n.
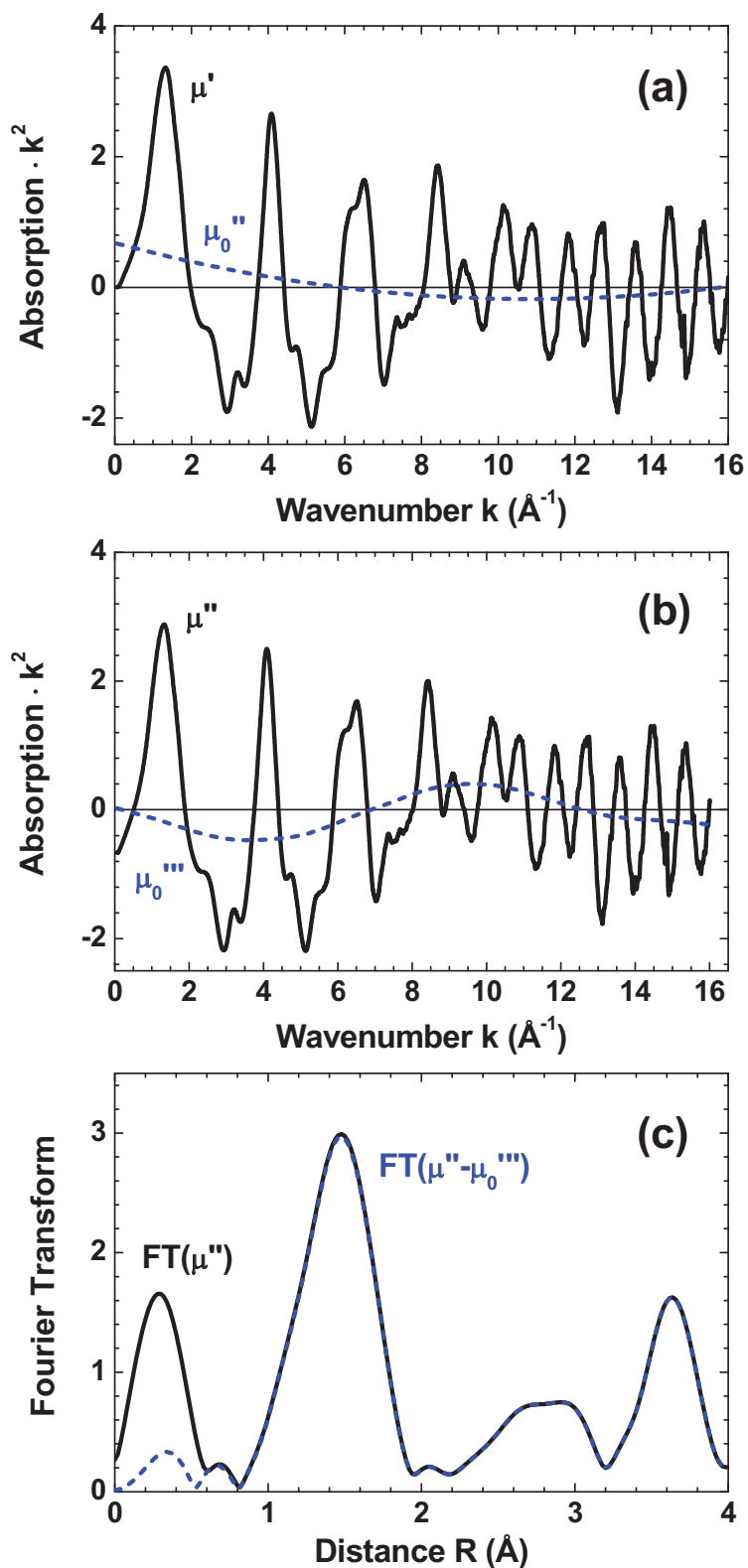
Figure 2.3: The second (a) and third (b) steps of zero-line removal. The Fourier transforms of the signals $\mu''(k)$ and $\mu''(k) - \mu_0'''(k)$ Note that the signal is multiplied by the factor $k^n, n = 2$. See text for details.

2.4 Fourier analysis of the EXAFS spectra

The EDAFT program allows one to carry out standard Fourier filtering procedure. The Fourier transform (FT) and back FT (BFT) are calculated according to the formulas

$$FT(R) = \sqrt{\frac{2}{\pi}} \int_{k_{\min}}^{k_{\max}} \chi(k) k^n W(k) \exp(-2ikR) dk \qquad (2.1)$$

$$BFT(k) = \frac{1}{k^n W(k)} \sqrt{\frac{2}{\pi}} \int_{R_{\min}}^{R_{\max}} FT(R) \exp(2ikR) dR \qquad (2.2)$$

where $k_{\min}$, $k_{\max}$ and $R_{\min}$, $R_{\max}$ denote, respectively, the ranges of the FT and BFT; $W(k)$ is a window function. Since the Fourier transform procedure is only correct for the integration in the infinite range while experimental signal is always limited by some interval, it is assumed that the signal goes to zero at $k \to \pm\infty$. To eliminate the abrupt behaviour of the signal at the ends of the measured interval (Fig. 2.4), the window function $W(k)$ is used. Five window functions are available [7]:

$$W(k) = 1$$
$$\text{(Rectangular)}, \qquad (2.3)$$

$$W(k) = J_0(\pi A \sqrt{1 - (1 - k/\bar{k})^2})/J_0(\pi A)$$
$$\text{(Kaiser} - \text{Bessel)}, \qquad (2.4)$$

$$W(k) = \exp(-0.5\pi A(1 - k/\bar{k})^2)$$
$$\text{(Gaussian)}, \qquad (2.5)$$

$$W(k) = \begin{cases} 0.025 + 0.5[1 - 0.95\cos(\pi(k - k_{\min})/A)] & \text{for } k < k_{\min} + A \\ 0.025 + 0.5[1 + 0.95\cos(\pi(k - k_{\max} + A)/A)] & \text{for } k > k_{\max} - A \\ 1.0 & \text{otherwise} \end{cases}$$
$$\text{(Hamming)}, \qquad (2.6)$$

$$W(k) = 0.045335 + 0.554883[1 - (1 - k/\bar{k})^2]^2 + 0.399782[1 - (1 - k/\bar{k})^2]^4$$
$$\text{(Norton} - \text{Beer F3)}, \qquad (2.7)$$

$$W(k) = \exp(-(k - \bar{k})^2/(\tilde{k}\ln(0.1)))$$
$$\text{(Gaussian } 10\%), \qquad (2.8)$$
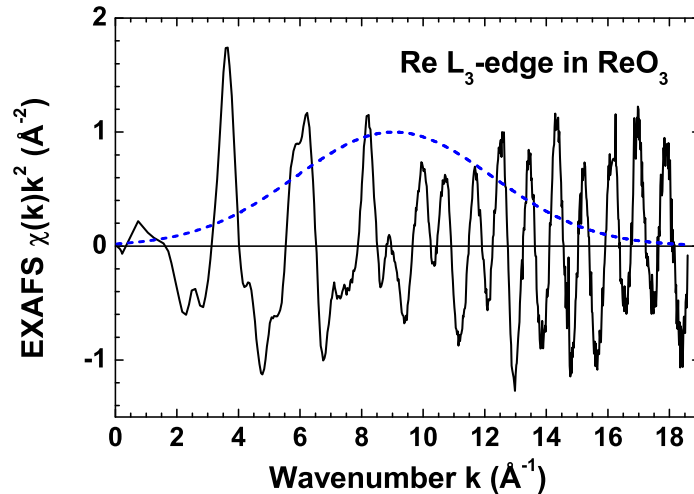
Figure 2.4: Experimental extended x-ray absorption fine structure (EXAFS) signal $\chi(k)k^2$ at the Re L_3-edge in ReO$_3$ (solid line) and the Gaussian-10% window function $W(k)$ (dashed line).

where A is the parameter of window, $J_0(x)$ is the Bessel function, $\bar{k} = (k_{\min} + k_{\max})/2$ and $\tilde{k} = (k_{\max} - k_{\min})/2$.

There are few useful functions which can be obtained after the FT and BFT procedures (Fig. 2.5). They are (1) the magnitude of FT

$$|FT(R)| = \sqrt{\Im(FT(R))^2 + \Re(FT(R))^2} \tag{2.9}$$

and (2) the amplitude ($AMPL(\chi(k))$) and phase ($PHASE(\chi(k))$) functions of the EXAFS signal which are useful to carry out the *amplitude ratio and phase difference* analyses [1]

$$AMPL(\chi(k)) = \sqrt{\Im(BFT(k))^2 + \Re(BFT(k))^2} \tag{2.10}$$

$$PHASE(\chi(k)) = \arctan\left(\Im(BFT(k))/\Re(BFT(k))\right) \tag{2.11}$$

where $\Im$ and $\Re$ denote the imaginary and real parts, respectively.

Recommendations

- Always use the same range in k-space both in the FT and BFT procedures.

- The best window is the one which produces the smallest distortion of the EXAFS signal after the FT and BFT procedures are applied. From our experience, the Kaiser-Bessel (equation (2.4)) and Gaussian (equation (2.5)) windows gives the best result in most cases (the values of the parameter A equal to ~1.5 and ~3.0 can be recommended for these two windows, respectively). However, try to use all types of windows and different values of the parameter A for any particular data to find the best solution.
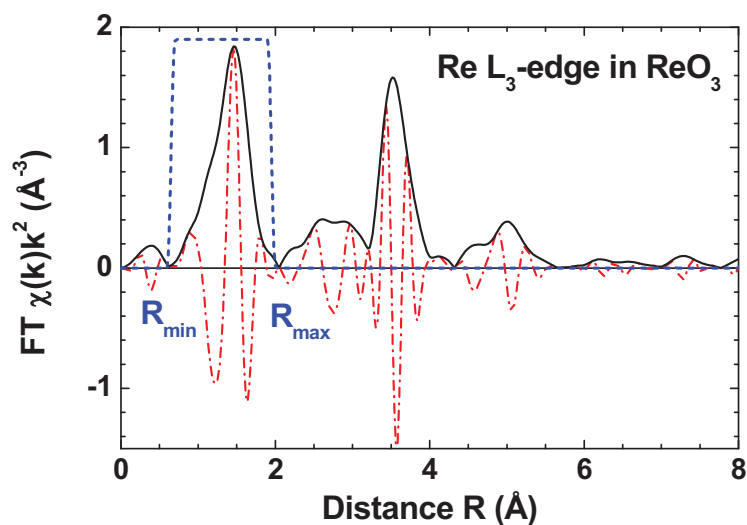
Figure 2.5: Fourier transform (FT) of the experimental EXAFS signal $\chi(k)k^2$ at the Re L$_3$-edge in ReO$_3$ (solid line – the modulus of FT, dash-dotted line – the imaginary part of FT) and the window function $W(k)$ used to set the range of the first coordination shell $[R_{\min}; R_{\max}]$ (dashed line).
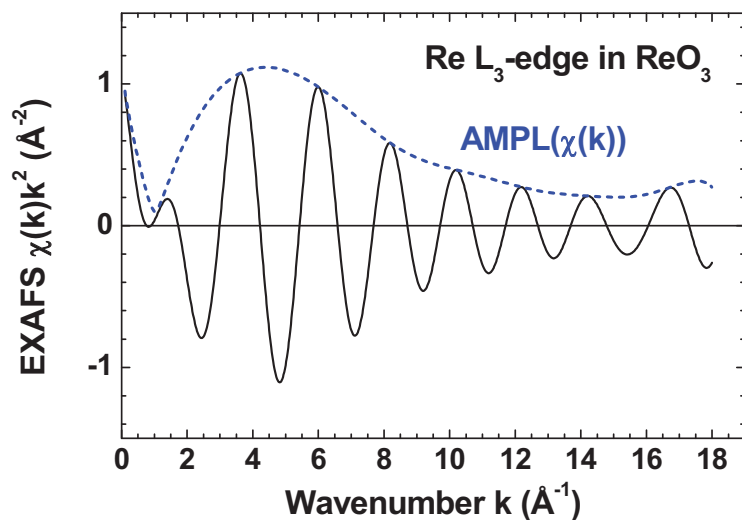
Figure 2.6: Back-Fourier transform (FT) (solid line) and the amplitude AMPL($\chi(k)$) of the EXAFS signal (dashed line).

2.5 Modelling of the EXAFS spectra within Gaussian and cumulant approximations

In the single-scattering curved-wave approximation an EXAFS signal $\chi(k)$ can be parameterized in the cumulant approximation

$$
\begin{aligned}
\chi_{model}(k) &= \sum_i^{shells} S_0^2 \frac{N_i}{kR_i^2} f_i(\pi, k, R_i) \exp(-2\sigma_i^2 k^2 + \frac{2}{3}C_{4i}k^4 - \frac{4}{45}C_{6i}k^6) \\
&\times \exp(-2R_i/\lambda(k)) \sin(2kR_i - \frac{4}{3}C_{3i}k^3 + \frac{4}{15}C_{5i}k^5 + \phi_i(\pi, k, R_i)) \quad (2.12)
\end{aligned}
$$

where $k = \sqrt{k^2 + (2m_e/\hbar^2)\Delta E_{0i}}$ is the photoelectron wave vector corrected for the difference ΔE_{0i} in the energy origin between experiment and theory; S_0^2 is the scale factor taking into account amplitude damping due to the multielectron effects; N_i is the coordination number of the i-shell; R_i is the radius of the i-shell; σ_i is the mean square radial displacement or Debye-Waller factor; C_{3i}, C_{4i}, C_{5i} and C_{6i} are cumulants of a distribution taking into account anharmonic effects and/or non-Gaussian disorder; $\lambda(k) = k/\Gamma$ (Γ is a constant) is the mean free path (MFP) of the photoelectron; $f(\pi, k, R_i)$ is the backscattering amplitude of the photoelectron due to the atoms of i-coordination shell; $\phi(\pi, k, R_i) = \psi(\pi, k, R_i) + 2\delta_l(k) - l\pi$ is the phase shift containing contributions from the absorber $2\delta_l(k)$ and the backscatterer $\psi(\pi, k, R_i)$ (l is the angular momentum of the photoelectron, l=1 for K and L_1 edges and l=2 or 0 for $L_{2,3}$ edges). The fitting parameters are $S_0^2 N_i$, R_i, σ_i^2, ΔE_{0i}, C_{3i}, C_{4i}, C_{5i}, C_{6i} and Γ.

The backscattering amplitudes $f(\pi, k, R_i)$ and phase shifts $\phi(\pi, k, R_i)$ have to be calculated theoretically, e.g. using the FEFF code [5], or extracted from experimental spectrum of reference compound. In the last case, the values of fitting parameters will be *relative*. If backscattering amplitude and phase shifts are calculated using a complex exchange and correlation potential, e.g. Hedin-Lundqvist type, the MFP is automatically included in the scattering amplitude, therefore Γ have to be set equal zero to eliminate $\exp(-2R_i/\lambda(k))$ term.

By setting $C_{3i} = C_{3i} = C_{5i} = C_{6i} = 0$ in equation (2.12), one obtains the Gaussian or harmonic approximation for the EXAFS signal

$$
\begin{aligned}
\chi_{model}(k) &= \sum_i^{shells} S_0^2 \frac{N_i}{kR_i^2} f_i(\pi, k, R_i) \exp(-2\sigma_i^2 k^2) \exp(-2R_i/\lambda(k)) \\
&\times \sin(2kR_i + \phi_i(\pi, k, R_i)). \quad (2.13)
\end{aligned}
$$

The radial distribution function (RDF) $G(R)$ corresponding to the equation (2.13) is

described by the Gaussian function

$$G(R) = \frac{N_i}{\sigma\sqrt{2\pi}} \exp\left(-\frac{(R-R_i)^2}{2\sigma_i^2}\right). \tag{2.14}$$

Note also that the EDAFIT program operates with the amplitude A_i of the EXAFS signal instead of N_i and S_0^2 separately. Therefore, $A_i = N_i S_0^2$ when the backscattering amplitude function $f(\pi, k, R_i)$ does not take into account S_0^2 factor; otherwise $A_i = N_i$.

To find values of the parameters describing an EXAFS spectrum, a non-linear least-squares fitting have to be performed. The function to be minimized is

$$S = \frac{1}{N} \sum_{i=1}^{N} (\chi_{exper}(k_i)k^n - \chi_{model}(a_1, ..., a_M, k_i)k^n)^2 \tag{2.15}$$

where N is the number of experimental points, M is the number of fitting parameters a_j and $M_{\max}$ is the maximum number of parameters (degrees of freedom) that can be determined from the data ranges Δk and ΔR used in the analysis. $M_{\max}$ is limited by the number of independent data points, and it is given by the Nyquist theorem [8, 9]

$$M_{\max} = \frac{2\Delta k \Delta R}{\pi}. \tag{2.16}$$

The results of a refinement can be evaluated using the covariance Cov and correlation Cor matrices defined as follows:

$$A(i,j) = \sum_{l=1}^{N} \frac{\partial \chi(k_l)}{\partial a_i} \frac{\partial \chi(k_l)}{\partial a_j}, \tag{2.17}$$

$$Cov = S_{\min} A^{-1}, \tag{2.18}$$

$$Cor(i,j) = \frac{Cov(i,j)}{\sqrt{Cov(i,i)Cov(j,j)}}, \tag{2.19}$$

where $S_{\min}$ is the minimum value of the sum of squares given by equation (2.15). The errors in the parameters can be estimated from the diagonal elements of the covariance matrix:

$$StDev(i) = \sqrt{Cov(i,i)}. \tag{2.20}$$

Minimization of the sum of squares (2.15) can be performed using different numerical algorithms among which the Newton-type procedures are now the most popular ones due to their fast convergence. However, the negative side of such algorithms is that they involve an inversion of large matrices, that can lead to the convergence difficulties, and sometimes the calculation of the second derivatives, that is time consuming. In the EDAFIT program, simple and efficient algorithm, which requires only the calculation of a model function and its first derivatives, is used. Its description is presented below.

Let us consider a standard least-squares problem

$$S = \sum_{i=1}^{n}(y_i - Y_i(x_1, ..., x_m))^2 \tag{2.21}$$

where $y_i, i = 1, ..., n$ is a set of experimental data and $Y_i(x_1, ..., x_m)$ is a model function depending on m parameters. The values of $x_j, j = 1, ..., m$, for which the sum (2.21) has a minimum, result from the solution of the system of m equations

$$\frac{\partial S}{\partial x_j} = 0 \quad or \quad \sum_{i=1}^{n}(y_i - Y_i)\frac{\partial Y_i}{\partial x_j} = 0, \quad j = 1, ..., m. \tag{2.22}$$

The model function Y_i can be expanded into the Tailor series

$$Y(x_j) = Y(x_j^0) + (x_j - x_j^0)\frac{\partial Y_i}{\partial x_j}(x_j^0) + ... \tag{2.23}$$

and substituted in the system of equations (2.22) by the first two terms of the series (2.23). After a few simple transformations, we obtain the expression for the jth parameter increment in the following form

$$\Delta x_j = x_j - x_j^0 = \frac{\sum_{i=1}^{n}(y_i - Y_i)\frac{\partial Y_i}{\partial x_j}}{\sum_{i=1}^{n}\left(\frac{\partial Y_i}{\partial x_j}\right)^2} \tag{2.24}$$

where x_j^0 denotes previous value of the jth parameter. This algorithm requires at each step only calculation of the model function and its first derivatives, which are found in the **EDAFIT** program analytically, and it is several times faster compared to commonly used Marquardt procedure. In the **EDAFIT** program, any parameter can be fixed to a constant or its range of values can be limited by the "hard wall" constraints.

An example of the best-fit procedure is given in Fig. 2.7.

Operational guide:

To use the **EDAFIT** program, one should prepare the input file as shown in Table 2.1. It consists of 43 lines containing the following information (see equation (2.12)):

Line 1: The number of shells. It can be up to 20.

Line 2: The maximum number of iterations ($I_{\max}$). The iteration process terminates when (1) the number of iterations exceeds $I_{\max}$, or (2) the increase of each parameter is less than its required *accuracy*, or (3) $(S_i - S_{i-1})/S_i \leq \epsilon$ (S is given by equation (2.15), and $\epsilon = 0.0001$).

Line 3: The first three numbers $k_{\min}$, $k_{\max}$ and Δk (in Å^{-1}) set the interval and the step between points in k-space (for EXAFS function). The fourth number (n) is the power of k used in the weighting factor k^n during the fit. The fifth number (*edge*)
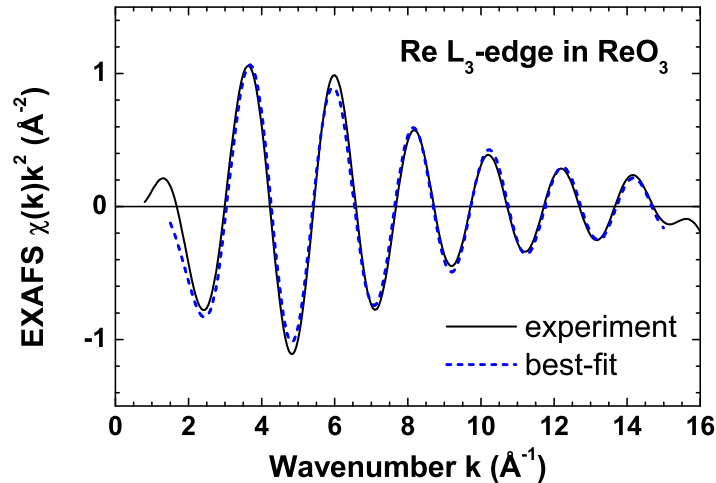
Figure 2.7: Comparison of the experimental EXAFS signal $\chi(k)k^2$ (solid line), obtained by isolating the first shell contribution using the back-FT procedure, with the best-fit calculated EXAFS signal (dashed line).

defines the type of the absorption edge: it is equal to 0 for K-edge, 1 for L_1-edge, 2 for L_2-edge and 3 for L_3-edge. The *edge* parameter affects the phase of the EXAFS signal, since it sets the value of l in equation (2.12): $l = 0$ for $edge = 0, 1$ and $l = 1$ for $edge = 2, 3$. Therefore, the value of *edge* must be consistent with the phase shift functions given in Line 4 and Line 39. N.B. If the central atom phase shift function contains the $(-l\pi)$ term, then always set *edge* to 2 or 3. The sixth number (*nexp*) is the power of k used in the weighting factor k^{nexp} of the experimental spectrum.

Line 4: The name of file with central atom phase shift $(2\delta_l(k))$.

Line 5: Parameter Γ (in Å^{-2}) used in the approximation of the mean free path in equation (2.12). The last three numbers correspond to the minimum and maximum limits ($\Gamma_{\min}$ and $\Gamma_{\max}$) and the required accuracy ($accuracy(\Gamma)$).

Lines 6,7,8,9: Amplitude (A_i), its limits ($A_{i_{\min}}$ and $A_{i_{\max}}$) and accuracy ($accuracy(A_i)$) for each i-shell.

Lines 10,11,12,13: Interatomic distance (R_i), its limits ($R_{i_{\min}}$ and $R_{i_{\max}}$) and accuracy ($accuracy(R_i)$) for each i-shell (in Å).

Lines 14,15,16,17: Debye-Waller factor (σ_i^2), its limits ($\sigma_{i_{\min}}^2$ and $\sigma_{i_{\max}}^2$) and accuracy ($accuracy(\sigma_i^2)$) for each i-shell (in Å^2).

Lines 18,19,20,21: Energy scale correction (ΔE_{0i}), its limits ($\Delta E_{0i_{\min}}$ and $\Delta E_{0i_{\max}}$) and accuracy ($accuracy(\Delta E_{0i})$) for each i-shell (in eV).

Lines 22,23,24,25: The third cumulant (C_{3i}), its limits ($C_{3i_{\min}}$ and $C_{3i_{\max}}$) and accuracy ($accuracy(C_{3i})$) for each i-shell (in Å^3).

Lines 26,27,28,29: The fourth cumulant (C_{4i}), its limits ($C_{4i_{\min}}$ and $C_{4i_{\max}}$) and accuracy ($accuracy(C_{4i})$) for each i-shell (in Å^4).

Lines 30,31,32,33: The fifth cumulant (C_{5i}), its limits ($C_{5i_{\min}}$ and $C_{5i_{\max}}$) and accuracy ($accuracy(C_{5i})$) for each i-shell (in Å^5).

Lines 34,35,36,37: The sixth cumulant (C_{6i}), its limits ($C_{6i_{\min}}$ and $C_{6i_{\max}}$) and accuracy ($accuracy(C_{6i})$) for each i-shell (in Å^6).

Line 38: The names of files with backscattering amplitude function ($f(\pi, k, R_i)$) for each i-shell.

Line 39: The names of files with backscattering phase shift function ($\psi(\pi, k, R_i)$) for each i-shell.

Line 40: The name of file with experimental first shell EXAFS spectrum.

Line 41: The name of file for calculated EXAFS spectrum.

Line 42: The name of file for output of auxiliary information about the fit.

Line 43: The name of file for calculated in the harmonic approximation RDF.

The value of any parameter can be fixed if one sets its *minimum* and *maximum* limits to the same number.

Recommendations

- Never use in a fit more parameters than it is allowed by the Nyquist theorem (equation (2.16)).

- Set starting values of parameters as close to their expected values as it is possible.

- Always choose likely values for the minimum and maximum limits of a parameter.

- Be sure that the iteration process converges to the *global* minimum. For this, try to run the program using different starting sets of parameters and allow one to do enough large number of iterations (usually about 50 iterations is good choice, however smaller or larger numbers can be used in some cases).

Table 2.1: Example of EDAFIT.INP file

2		number of shells
20		number of iterations
1 14 0.05 2 3 1		$k_{\min}, k_{\max}, \Delta k, n, edge, nexp$
cph.dat		central atom phase shift
0.0 0.0 0.0 0.00001		$\Gamma, \Gamma_{\min}, \Gamma_{\max}, accuracy(\Gamma)$
6	6	A
1	1	$A_{\min}$
7	8	$A_{\max}$
0.00001	0.00001	$accuracy(A)$
1.9	3.8	R
1.0	3.0	$R_{\min}$
2.0	4.2	$R_{\max}$
0.0000001	0.0000001	$accuracy(R)$
0.002	0.004	σ^2
0.0	0.0	$\sigma^2_{\min}$
0.05	0.05	$\sigma^2_{\max}$
0.00000001	0.00000001	$accuracy(\sigma^2)$
0	0	ΔE_0
-10.0	-10.0	$\Delta E_{0_{\min}}$
10.0	10.0	$\Delta E_{0_{\max}}$
0.01	0.01	$accuracy(\Delta E_0)$
0.0	0.0	C_3
0.0	0.0	$C_{3_{\min}}$
0.0	0.0	$C_{3_{\max}}$
0.0001	0.0001	$accuracy(C_3)$
0.0	0.0	C_4
0.0	0.0	$C_{4_{\min}}$
0.0	0.0	$C_{4_{\max}}$
0.0001	0.0001	$accuracy(C_4)$
0.0	0.0	C_5
0.0	0.0	$C_{5_{\min}}$
0.0	0.0	$C_{5_{\max}}$
0.0001	0.0001	$accuracy(C_5)$
0.0	0.0	C_6
0.0	0.0	$C_{6_{\min}}$
0.0	0.0	$C_{6_{\max}}$
0.0001	0.0001	$accuracy(C_6)$
amp1.dat	amp2.dat	backscattering amplitudes
pha1.dat	pha2.dat	backscattering phase shifts
reo3e.txt		experimental EXAFS spectrum
xt.txt		calculated EXAFS spectrum
fit.dat		file with additional information about the fit
rdf.txt		calculated in the harmonic approximation RDF

- In the case of one shell fit, a good practice is to calculate the correlation matrix (it can be done at the end of the fitting process). It gives an information about the error bars of obtained parameters. However, one should remember that these error bars are only related to the errors of the fit but not to the *total* error which includes also the part due to the differences in experimental spectra measured at different experimental conditions (e.g. storage ring current, crystal monochromator, sample thickness, temperature instabilities, etc.). Therefore, obviously, the *total* error bar of any parameter will be *greater* than the one estimated from the correlation matrix.

- If the experimental data are available in a large enough range of wave vectors (e.g. from 0 to 16 Å^{-1}), try to fit them choosing different fitting intervals (e.g. 0–16 Å^{-1} or 1–15 Å^{-1} or 2–14 Å^{-1}). This can be useful to estimate the influence of the Fourier transform procedure if it was used.

2.6 Modelling of the EXAFS spectra using regularization like method

The EDARDF program allows one to determine *model independent* radial distribution function (RDF) using theoretical or experimental backscattering amplitudes and phase shifts. The method implemented in the EDARDF program is especially suitable for the analysis of the first coordination shell XAFS signal in *highly locally* disordered materials, as amorphous compounds, glasses, low-symmetry crystals and systems with highly anharmonic behaviour, where the cumulant approach fails [10]. However, the method works with the same success in the case of crystalline materials [11]. The idea of the method is as follows.

The general expression for the XAFS $\chi(k)$ in terms of the distribution functions can be written as [12]

$$
\begin{aligned}
\chi(k) \;=\; & \int 4\pi R^2 \rho_0 g_2(R)(\chi_2^{oio}(k) + \chi_4^{oioio}(k) + \ldots)\mathrm{d}R \\
& + \iiint 8\pi^2 R_1^2 R_2^2 \sin(\theta)\rho_0^2 g_3(R_1, R_2, \theta) \\
& \times (2\chi_3^{oijo}(k) + 2\chi_4^{oiojo}(k) + \chi_4^{oijio}(k) + \chi_4^{ojijo}(k) + \ldots)\mathrm{d}R_1 \mathrm{d}R_2 \mathrm{d}\theta \\
& + \iiiiii 8\pi^2 R_1^2 R_2^2 R_3^2 \sin(\theta)\rho_0^3 g_4(R_1, R_2, \theta, R_3, \Omega) \\
& \times (2\chi_4^{oijko}(k) + 2\chi_4^{oikjo}(k) + 2\chi_4^{ojiko}(k) + \ldots)\mathrm{d}R_1 \mathrm{d}R_2 \mathrm{d}\theta \mathrm{d}R_3 \mathrm{d}\Omega \\
& + \ldots \qquad\qquad\qquad\qquad\qquad\qquad\qquad\qquad\qquad\qquad (2.25)
\end{aligned}
$$

where ρ_0 is the average density of a system and $\chi_m(k)$ are the multiple-scattering XAFS

signals of the $(m-1)$ order generated within a group of atoms (o, i, j, k, ...) described by g_n.

Further we will be interested only in the first coordination shell XAFS signal. We will consider a system with the first shell containing only one type of atoms and being well separated from others so that its XAFS signal can be easily singled out by the Fourier filtering technique. In reality the range of materials, which meet to above condition, is very wide although some exceptions (e.g. liquids, some organic materials) occur where the first shell overlap strongly with the outer ones. Note that the first shell XAFS signal does not usually contain any high-order scattering contributions due to that only the first integral in the expression (2.25) can be taken into account.

The following formalism will be given in terms of the radial distribution function (RDF) $G(R) = 4\pi R^2 \rho_0 g_2(R)$ which corresponds to the number of atoms located in the spherical shell around the photoabsorber between R and $R+dR$. Thus the average number N of atoms located in the region between $R_{\min}$ and $R_{\max}$ is given by the integral

$$N = \int_{R_{\min}}^{R_{\max}} G(R) dR \tag{2.26}$$

and is called the coordination number.

From (2.25), the first shell XAFS for an arbitrary RDF $G(R)$ is given within the spherical-wave approximation (SWA) by

$$\chi(k) = S_0^2 \int_{R_{\min}}^{R_{\max}} \frac{G(R)}{kR^2} F(\pi, k, R) \sin(2kR + \Phi(\pi, k, R)) dR \tag{2.27}$$

where S_0^2 is the scale factor taking into account amplitude damping due to the multielectron effects; R is the interatomic distance; $F(\pi, k, R)$ is the backscattering amplitude of the photoelectron due to the atoms located at the distance R from the photoabsorber and $\Phi(\pi, k, R) = \psi(\pi, k, R) + 2\delta_l(k) - l\pi$ is the phase shift containing contributions from the photoabsorber $2\delta_l(k)$ and the backscatterer $\psi(\pi, k, R)$ (l is the angular momentum of the photoelectron, $l=1$ for the K and L_1 edges and $l=2$ or 0 for the $L_{2,3}$-edges). In the present notation the amplitude function $F(\pi, k, R)$ contains intrinsic the damping factor due to the mean free path of the photoelectron assuming that $F(\pi, k, R)$ is calculated using a complex exchange-correlation potential of Hedin-Lundqvist type [13].

Among different approaches to the XAFS data analysis, there is one very promising method based on the regularization technique [14]. It solves the integral equation describing the XAFS as an ill-posed problem using the regular algorithm and allows one to reconstruct the model-independent distribution function $g_2(R)$. The idea of the method is to find $g(R)$ minimizing the functional [14]

$$\|\chi_{\mathrm{model}}(k) - \chi_{\mathrm{exp}}(k)\|^2 + \alpha \int_{R_{\min}}^{R_{\max}} |g(R)|^2 dR + \beta \int_{R_{\min}}^{R_{\max}} \left|\frac{dg(R)}{dR}\right|^2 dR \tag{2.28}$$

where the regularization parameters α and β are small and positive. The presence of the terms with α and β makes the problem stable and solvable using the methods of linear algebra (the Gauss method, the square-root method, etc. [15, 14]) used for the inversion of the matrix related to the system of linear algebraic equations arising on the equality to zero of the derivatives of the functional (2.28). The term with α accounts for the normalization condition of $g(R)$ while the term with β realizes the condition of its smoothness. Note that the regularization method is stable to the size of the interval in k-space used in the analysis [14]. The disadvantage of the method is the need to choose the regularization parameters α and β whose "bad" values lead to neither the problem (2.28) becomes unsolvable or the obtained $g(R)$ gives the XAFS signal $\chi_{\mathrm{model}}(k)$ which differs strongly from the experimental XAFS $\chi_{\mathrm{exp}}(k)$. It is known [15] that when α and β tend to zero, the requirement of closeness between the model and experimental XAFS signals $\chi_{\mathrm{model}}(k) \rightarrow \chi_{\mathrm{exp}}(k)$ realizes analogous to the least-squares method. On practice, the values of α and β are enough small ($\sim 10^{-6} - 10^{-7}$ [14]) so that the contribution of the last two terms in (2.28) is also small compared to the one of the first term.

In the **EDARDF** program, the following approach to the determination of $G(R)$ is suggested. Using the fact that α and β are small quantities, we will set them to zero and transform the functional (2.28) into the standard least-squares problem for the XAFS function $\chi(k)$

$$\|\chi_{\mathrm{model}}(k) - \chi_{\mathrm{exp}}(k)\|^2 \tag{2.29}$$

which is solved iteratively with an additional requirement on the smoothness of $G(R)$ (see below). The normalization condition for $G(R)$ (equivalent to the one given by the term with α in (2.28)) can be also imposed if required by re-scaling procedure applying to $G(R)$ at every iteration, however, on practice, it is often unnecessary due to the presence of the S_0^2 scaling factor in (2.27) which is usually known with an accuracy about 10 %.

The iterative procedure can be realized using different numerical algorithms among which the Newton-type procedures are now the most popular ones due to their fast convergence. However, the negative sides of such algorithms are that first, they involve an inversion of large matrices, that can lead to the convergence difficulties, and, second, a calculation of the second derivatives is sometimes time consuming. Here it is solved using the same algorithm as described in section 2.5 (equation (2.24)).

The starting approximation for $G(R)$ in (2.27) can be chosen as, for example, a Gaussian given on the grid from R_{min} to R_{max} with a step $\mathrm{d}R$ related to the spatial resolution δR (see below for detail). The amplitude of $G(R)$ is allowed one to vary at every iteration in each small interval $\mathrm{d}R$ till good agreement between experimental and model XAFS signals will be reached. Additionally, the criterion of smoothness is applied to $G(R)$. It

allows one to eliminate non physical behaviour of $G(R)$ as breaks, sharp needle-like peaks, etc. The criterion is realized using standard non-linear 7-point smoothing algorithm based on the third-order polynomial function. The smoothing is carried out at each step of the iteration procedure continuously keeping the smooth shape of the RDF during the fit.

The XAFS function $\chi(k)$ and the RDF $G(R)$ are related each other via the integral equation (2.27) therefore if $\chi(k)$ is given in k-space from 0 to $k_{\max}$ with a step $\mathrm{d}k$, $G(R)$ is given in R-space from 0 to $R_{\max} \simeq \pi/2\mathrm{d}k$ with the spatial resolution $\delta R = 1/2k_{\max}$ (e.g. $\delta R \simeq 0.03$ Å for $k_{\max} = 16$ Å^{-1}) [16, 17]. The value of δR gives an estimate for the step $\mathrm{d}R$ used in (2.27): the later should be smaller than the spatial resolution δR otherwise the information containing in $\chi(k)$ can be loosed, but, at the same time, it should be enough large to allow the convergence and stability of the fitting procedure. Note also that the use of a little bit smaller value of $\mathrm{d}R$ than it is given by δR is possible due to the smoothness criterion which imposes an additional constrain on the shape of the RDF $G(R)$. The experience shows that the value of $\mathrm{d}R = 0.01 - 0.02$ Å can be used in most cases.

Operational guide:

To use the EDARDF program one should create an input file, e.g. called EDARDF.INP (see Table 2.2). It has the ASCII format and consists of 13 lines containing required information:

Line 1: The maximum number of iterations which defines the end of the fitting process.

Line 2: The first three numbers $k_{\min}$, $k_{\max}$ and Δk (in Å^{-1}) set the interval and the step between points in k-space (for EXAFS function). The fourth number (n) is the power of k used in the weighting factor k^n. It should be the same as for experimental spectrum. The fifth number ($edge$) defines the type of the absorption edge: it is equal to 0 for K-edge, 1 for L$_1$-edge, 2 for L$_2$-edge and 3 for L$_3$-edge. The $edge$ parameter affects the phase of the EXAFS signal, since it sets the value of l in equation (2.12): $l = 0$ for $edge = 0, 1$ and $l = 1$ for $edge = 2, 3$. Therefore, the value of $edge$ must be consistent with the phase shift functions given in Line 3 and Line 8. N.B. If the central atom phase shift function contains the $(-l\pi)$ term, then always set $edge$ to 2 or 3. The sixth number ($nexp$) is the power of k used in the weighting factor k^{nexp} of the experimental spectrum. The last two numbers $R_{\min}$ and $R_{\max}$ (in Å) set the interval in R-space for the RDF function.

Line 3: The name of the file with the central atom phase shift.

Line 4: The value of the E_0 correction (in eV).

Line 5: The names of the files with the backscattering amplitude functions.

Line 6: The names of the files with the backscattering phase shift functions.

Line 7: The distance r_{sep} (in Å) separates two ranges of the RDF $G(R)$ if two backscattering amplitude and phase shift functions are specified at Line 5 and 6. It is not used if only one amplitude/phase shift function is given.

Line 8: The name of the file with the experimental first-shell EXAFS spectrum.

Line 9: The name of the file for the calculated EXAFS spectrum.

Line 10: The name of the file for auxiliary information about the fit.

Line 11: The name of the file for calculated RDF $G(R)$.

Table 2.2: Example of EDARDF.INP file

20	number of iterations
2 13 0.05 2 3 2 0.8 2.6	$k_{\mathrm{min}}, k_{\mathrm{max}}, \Delta k, n, edge, nexp, R_{\mathrm{min}}, R_{\mathrm{max}}$
cph.dat	central atom phase shift
0.0	ΔE_0
amp1.dat amp2.dat	backscattering amplitudes $f(\pi, k, r)$
pha1.dat pha2.dat	backscattering phase shifts $\psi(\pi, k, r)$
1.9	r_{sep}
reo3e1.txt	experimental first shell EXAFS spectrum
xt.txt	calculated EXAFS spectrum
fit.dat	file with additional information about the fit
rdf.txt	calculated RDF

When the EDARDF program starts, one should enter the name of the input file (as EDARDF.INP) and specify starting approximation for the RDF. The shape of the RDF can be set in two different ways in the form of:

1. a Gaussian distribution given on the grid from R_{min} to R_{max} (the grid step and the position of the maximum of the distribution are defined by user);

2. an arbitrary distribution given on an uniformly spaced grid in a file (thus the output RDF can be used as the input one for the following fits).

During the fitting process, the EDARDF program shows calculated and experimental EXAFS spectra and their residual, the RDF before and after smoothing and the error reflecting disagreement between calculation and experiment.

Estimation of the results:

The RDF $G(R)$ calculated during the fitting process can be directly compared with the ones obtained by other experimental techniques or during the computer simulations as molecular dynamics and Monte Carlo method. However, it is often useful for comparison with the results of other techniques to have a set of structural parameters but not a total distribution function. Therefore a parametrization of the obtained RDF using a proper analytical model can be done. In the simplest case, a decomposition into a set of Gaussians can be performed leading to the results close to the ones which can be obtained by the standard multi-shell least-squares fitting approach. However, if the RDF has strongly asymmetric shape, more complicated analytical form than Gaussian should be used. It is necessary to point out that if parametrization is performed, one have to take into account the total number of parameters used in the model: it must be less than the one given by the Nyquist theorem [8, 9]

$$M_{\max} = \frac{2\Delta k \Delta R}{\pi} \tag{2.30}$$

where Δk and ΔR are respectively the widths in k and R space used in the fit (for example $M_{\max} \simeq 11.5$ at $\Delta k = k_{\max} - k_{\min} = 15$ Å^{-1} and $\Delta R = R_{\max} - R_{\min} = 1$ Å).

Recommendations

- Do not use the EDARDF program for experimental data with large noise.

- Do not use too small or too big step in R-space. The optimum value of ΔR seems to be $\sim 0.01 - 0.02$ Å, however check different values for each particular case.

- If ΔE_0 is allowed to be varied (this is only the case when $\Delta E_{0_{\min}} < \Delta E_{0_{\max}}$), the calculation takes much longer time, therefore try to choose its value close to the correct one manually and fix it.

Examples of the EDARDF *application*
and its comparison with other methods:

Here the application of the EDARDF program is presented and compared with other commonly used techniques (the multi-shell fit, the cumulant approach and the splice technique) on the example of model distributions and experimental data for ReO$_3$, WO$_3$ and α-MoO$_3$ [2]. The four methods are considered: the Gaussian or harmonic approximation (method 1), the cumulant approach (up to the fourth cumulant) (method 2), the method described above (EDARDF) (method 3) and the splice technique (method 4). First, to compare the methods 1, 2 and 3, the four distribution functions shown in Fig. 2.8 by

dotted lines were chosen to cover all range of possible RDF shapes having different degree of distortion and asymmetry frequently occurring in real situations. The first distribution (Fig. 2.8(a)) corresponds to the simplest case of one Gaussian centred at 1.8 Å with the width $\sigma = 0.05$ Å. The second distribution (Fig. 2.8(b)) consists of two slightly separated Gaussians at 1.8 Å and 1.9 Å with the ratio of amplitudes 2:1 and equal widths $\sigma = 0.05$ Å. The third distribution (Fig. 2.8(c)) consists of two strongly separated Gaussians at 1.8 Å and 2.1 Å with the ratio of amplitudes 2:1 and slightly different widths $\sigma = 0.05$ and 0.06 Å. The fourth distribution (Fig. 2.8(d)) represents the case of strongly asymmetric non-Gaussian distribution with a long tail frequently observed in superionic materials.

The XAFS signal $\chi_{\text{sim}}(k)$ was simulated for each distribution using expression (2.27) with $S_0^2 = 1$ and the backscattering amplitude $F(\pi, k, R)$ and phase shift $\Phi(\pi, k, R)$ functions for Cu–O atom pair. The $F(\pi, k, R)$ and $\Phi(\pi, k, R)$ functions were calculated theoretically by the FEFF code [4, 5]. Thus obtained XAFS signals $\chi_{\text{sim}}(k)$ were fitted in the range $\Delta k = 1 - 16$ Å^{-1} using the methods 1, 2 and 3 till the best agreement between $\chi_{\text{sim}}(k)$ and $\chi_{\text{fit}}(k)$ was found. Based on the results of the fit, the RDFs were obtained and compared with the model ones. Note that in the case of the method 3, the RDF $G(R)$ is the output result whereas it should be constructed for the methods 1 and 2. The RDF in the method 1 is given by a Gaussian or a sum of Gaussians calculated from a set of structural parameters (N, R, σ) obtained during the fit. In the case of the method 2, the RDF can be found by the procedure described in [21, 22].

The RDFs obtained by the methods 1, 2 and 3 are compared with the original model distributions in Fig. 2.8. As one can see, all three methods reproduce rather well the simplest model (Fig. 2.8(a)). Here the observed differences are only due to the fitting errors.

The method 1 works also excellent in the case of the multi-peak Gaussian models (Fig. 2.8(b) and (c)) being able to reconstruct the RDF in both cases when Gaussians are spread closely or far away. However, this method fails completely in attempt to reproduce strongly asymmetric distribution (Fig. 2.8(d)): It is clearly visible that the obtained RDF differs significantly from the model RDF both in the position and in the shape of the distribution.

Opposite to the method 1, the cumulant approach (method 2) fails in the case of the Gaussian distributions splitted into two components (Fig.s 2.8(b) and (c)): It gives the more error the larger splitting occurs. However, the method 2 works well when distribution remains single-peak shaped but becomes strongly asymmetric (Fig. 2.8(d)). This result is not surprising since the cumulant approach was developed for the analysis of systems with *moderate* disorder [19, 20, 21, 22] whose RDFs deviate slightly from Gaussianity. More precise criterion is that the cumulant approach can be used in such cases when
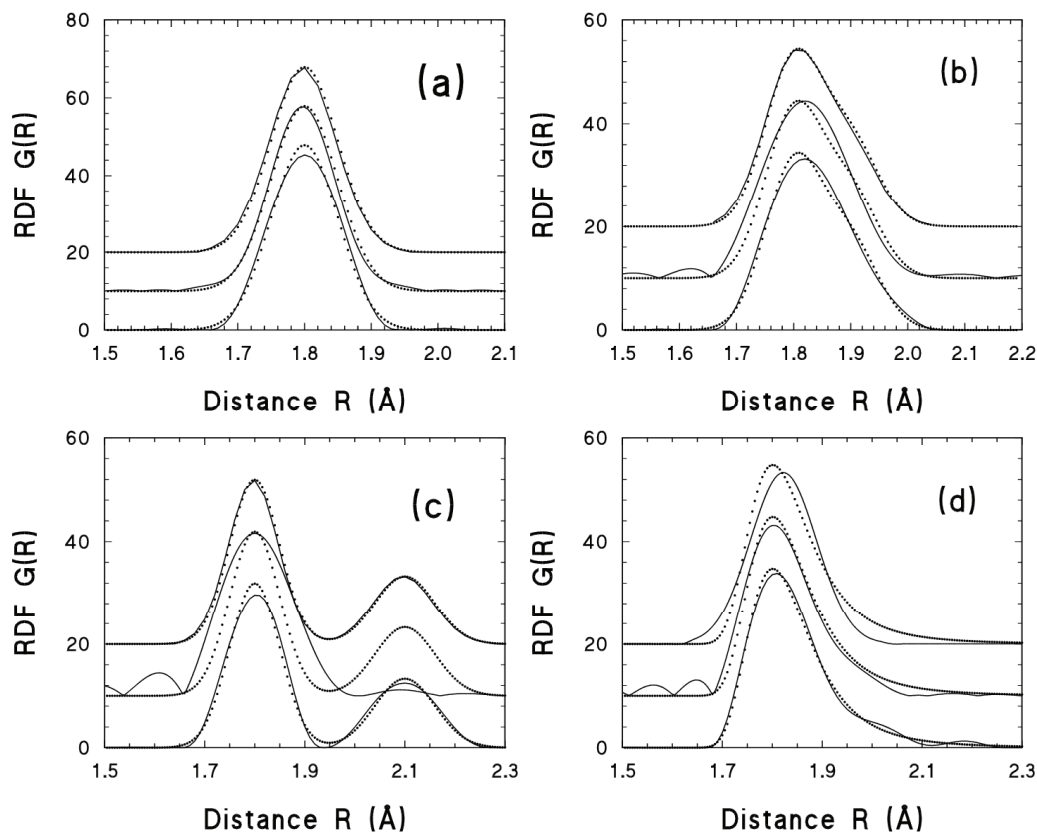
Figure 2.8: The RDFs derived by different methods (the Gaussian approximation (upper solid curves), the cumulant approximation (middle solid curves) and the model-independent approach suggested in the present work (lower solid curves)) are compared to the model RDFs (dotted lines): (a) single Gaussian model; (b) double-Gaussian model with the Gaussian separation $\Delta R = 0.1$ Å; (c) double-Gaussian model with the Gaussian separation $\Delta R = 0.3$ Å; (d) asymmetric model.

the expansion of the logarithm of the "effective" distribution Fourier transform results in rapidly convergent series [19, 20, 21].

Thus both Gaussian (method 1) and cumulant (method 2) approximations have limited ranges of applicability. Note also that in spite of the latter is claimed to be the model-independent approach, it is only able to reproduce distribution functions with strongly restricted shape.

The method 3 described above (EDARDF) gives good agreement between original and reconstructed RDFs in all cases independently on whether distortion or asymmetry is present or not. An additional illustration of the application of the method 3 to two model distributions is shown in Fig. 2.9. Also in this case the obtained agreement between the starting model and the obtained RDF is good. Note that small discrepancy between shapes of the model and obtained RDFs, which can be seen in Figs. 2.8 and 2.3, is due to
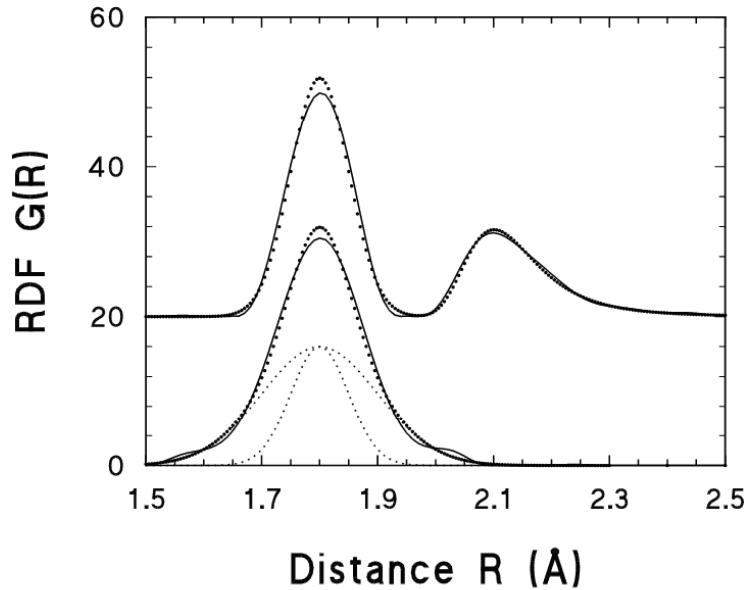
Figure 2.9: The RDFs reconstructed by the method suggested in the present work (solid curves) in comparison with the model RDFs (dotted lines): the mixed Gaussian-asymmetric double-peak model (upper curve) and the double-Gaussian model (lower curve) with the Gaussians (shown by dots) centred at $R=1.80$ Å and having the amplitudes (N) and the widths (σ) equal to $N_1 = 2$, $\sigma_1 = 0.05$ Å and $N_2 = 4$, $\sigma_2 = 0.10$ Å, respectively.

the limited range ($\Delta k = 1 - 16$ Å^{-1}) of the XAFS signal used in the fit: Such limitation leads to the decrease of the spatial resolution and thus affects the shape of the obtained RDF in the way similar to the convolution with a Gaussian.

Further we compare the method 3 (EDARDF) with another model-independent approach - the splice technique [17, 18], mentioned above as the method 4. The calculations within the splice approach were done according to [17, 18]: the low-k region of the XAFS signal $\chi(k)$ was reconstructed using cumulant expansion and the RDF G(R) was obtained by the Fourier transform

$$G(R) = -(R^2/S_0^2)\text{Im} \int_0^{k_{\max}} k\chi(k)\frac{\exp(-i\Phi(\pi, k, R))}{F(\pi, k, R)} \exp(-2ikR)\mathrm{d}k. \qquad (2.31)$$

A number of limitations of the splice technique were already discussed in [17], however one should point out an additional problem occurring frequently on practice. It is related to the upper limit $k_{\max}$ of the XAFS signal $\chi(k)$ available from an experiment. Formally the RDF $G(R)$ can be obtained from $\chi(k)$ using equation (2.31) with $k_{\max}$ set to infinity. In reality, the experimental XAFS signal is given within an interval from $k_{\min}$ to $k_{\max}$. It can be extrapolated in the low-k region for a number of systems using the cumulant expansion [17] however the high energy information on $\chi(k)$ at $k > k_{\max}$ is anyway lacking. In [17], it is stated that the upper limit $k_{\max}$, given by the backscattering amplitude function

$F(\pi, k, R)$ decreasing at high-k values into the noise, is not a serious limitation since its main effect is to restrict the spatial resolution δR. However, it is easy to see that since the integral in (2.31) is calculated from the XAFS signal $\chi(k)$ corrected both on the backscattering amplitude and phase functions and on the wave vector k, the integration depends only on the behaviour of the reduced $\chi'(k)$ signal which is the oscillatory quantity modulated by the RDF $G(R)$. In the simplest case of the Gaussian disorder, the amplitude of $\chi'(k)$ decreases as $\exp(-2\sigma^2 k^2)$. Thus, if the values of $\chi'(k)$ are not negligible at $k > k_{\max}$ (note that $\chi'(k)$ does not depend on the backscattering amplitude as well as on the backscattering phase !), a part of the information on the RDF is missed and consequently the shape of $G(R)$ obtained from (2.31) is wrong. Moreover, if $\chi'(k)$ deviates strongly from zero at $k = k_{\max}$, an additional noise in the $G(R)$ occurs due to the so-called *truncation* effect [16] leading to the appearing in the RDF of a set of harmonics at both sides of every structural peak. A criterion for the estimation of the $k_{\max}$ value, which is sufficient to have for the reliable use of the splice technique, in the case of the Gaussian disorder, characterized by the width σ, can be derived from

$$\exp(-2\sigma^2 k_{\max}^2) = \frac{A(k = k_{\max})}{A(k = 0)} \tag{2.32}$$

where $A(k = 0)$ and $A(k = k_{\max})$ correspond to the maximum amplitude of $\chi'(k)$ at $k = 0$ and $k = k_{\max}$, respectively. If one takes $A(k = k_{\max})/A(k = 0) = 0.01$, that means enough small value of $A(k = k_{\max})$ to consider the value of the integral in (2.31) at $k > k_{\max}$ to be negligible and the truncation effect to be small, then $k_{\max} = 30$ Å^{-1} for $\sigma = 0.05$ Å and $k_{\max} = 15$ Å^{-1} for $\sigma = 0.10$ Å.

The sensitivity of the method 3 and the splice approach (method 4) to the upper limit $k_{\max}$ of the XAFS signal is well illustrated in Fig. 2.10 on the example of the model RDF – the same as in Fig. 2.8(c). The simulated XAFS signal $\chi_{\text{sim}}(k)$ was used in the ranges from $k_{\min} = 0$ Å^{-1} to $k_{\max} = 8, 10, 12$ and 16 Å^{-1}. It is clearly visible in Fig. 2.10 that the splice method is strongly sensitive to the upper limit of the XAFS signal: the shorter is the range of $\chi'(k)$ the larger difference is present between the model (dotted lines) and obtained (dashed lines) RDFs. On the contrary, the method 3 shows much smaller sensitivity to the $k_{\max}$ value. Such result can be readily understood from the analysis of the form of the equations (2.27) and (2.31) on which the methods are based. The error occurring in the splice approach is directly related to the limited range of the XAFS function or, more precisely, to the fact that the reduced XAFS signal $\chi'(k)$ is enough big at $k = k_{\max}$ that lead to (1) the value of the integral in (2.31) at $k > k_{\max}$ is not negligible and (2) the additional noise due to the truncation effect appears when $k_{\max}$ decreases. In the method 3, the integrant function in (2.27) is going to zero at both ends ($R_{\min}$ and $R_{\max}$) of the first shell interval thanks to the RDF $G(R)$ becoming negligibly small.
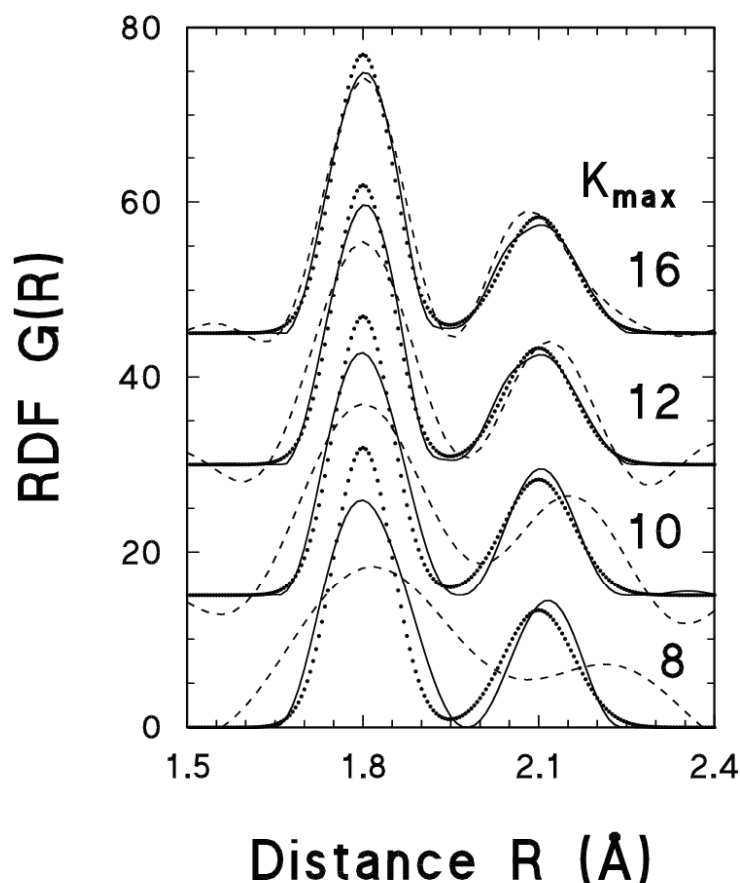
Figure 2.10: The RDFs obtained by the method 3 (solid line) and by the splice method 4 (dashed line) are compared to the double-Gaussian model RDF shown by dotted line. Influence of the high wave vector limit $k_{\max}$ used in the analysis on the shape of the obtained RDFs is clearly visible.

One should point out that $G(R)$ has such favourable behaviour only when the first shell is separated from the outer ones that is in many crystalline, amorphous and glass-like solids. In the case of, for example, liquid metals [23, 24], the first shell cannot be singled out therefore the method 3 as presented above will fail. However, it seems promising that the modified approach, which takes into account the long-distance behaviour of $G(R)$, will cover also this class of materials.

Further the application of the methods 3 and 4 to three crystalline materials ReO_3, WO_3 and α-MoO_3 will be discussed (Fig. 2.11). The peculiarity of the considered compounds is that they have the first shell around metal atom consisting of six oxygens but having different degree of distortion. In cubic ReO_3 [25], the oxygen atoms form a regular octahedron so only one peak should be observed in the RDF (upper panel in Fig. 2.12). In monoclinic WO_3 [26], the oxygen octahedra are distorted and there are also two non-equivalent tungsten atom sites in the unit cell therefore a spread of twelve W–O distances
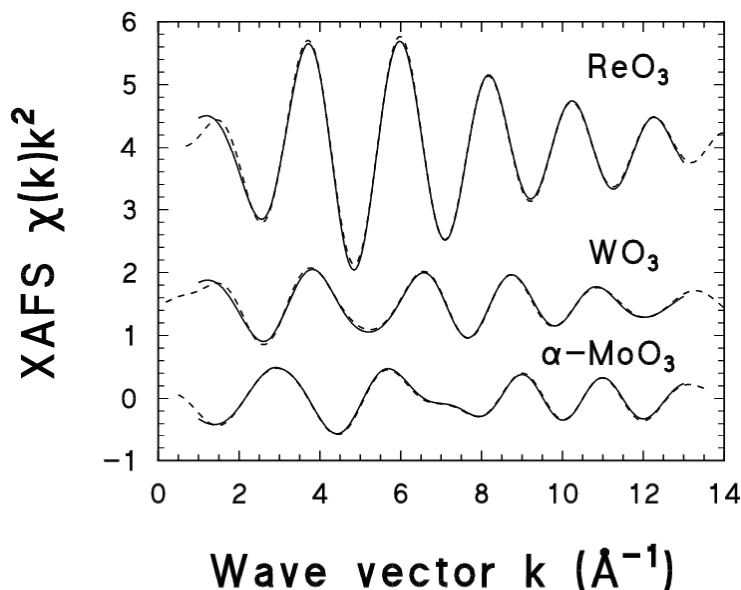
Figure 2.11: The first shell XAFS signals $\chi(k)k^2$ obtained by the method 3 (solid lines) in comparison with the experimental ones (dashed lines) for the Re L_3-edge in ReO_3, the W L_3-edge in WO_3 and the Mo K-edge in α-MoO_3.

from 1.73 Å to 2.18 Å, which can be separated into six groups, is present leading to the double-peak shape of the RDF (middle panel in Fig. 2.12). In orthorhombic α-MoO_3 [27], the distortion of the oxygen octahedron is the largest one due to the presence of very short ($R(Mo=O) = 1.67$ Å) and long ($R(Mo—O) = 2.33$ Å) bonds. As a result, there are three groups of the Mo–O distances and the RDF around molybdenum atom has the triple-peak shape (lower panel in Fig. 2.12).

The first shell XAFS signals $\chi(k)k^2$, obtained by the method 3 (solid lines), are compared to the experimental ones (dashed lines) in Fig. 2.11. Good agreement between the calculated and experimental XAFS signals is observed. The analysis was done in the range $\Delta k = 1 - 13$ Å^{-1}. The RDFs $G(R)$, corresponding to the calculated signals $\chi(k)k^2$, are presented by solid lines in Fig. 2.12 where the RDFs, obtained for the same materials by the method 4 (the splice technique), are also shown by dotted lines. The agreement between the results obtained by both methods is good as well as with diffraction data shown in Fig. 2.12 by dashed lines. Such artefacts as the negative values of the RDFs obtained by the splice method are due to the limited range of the available experimental XAFS signal. Note that except structural peaks, there is a number of non-structural peaks which are mainly present at short distances $R < 1.5 - 1.7$ Å. These peaks correspond to the low-frequency signals whose origin is due to the atomic-like oscillations [28] and to the errors of the XAFS zero-line removal procedure.
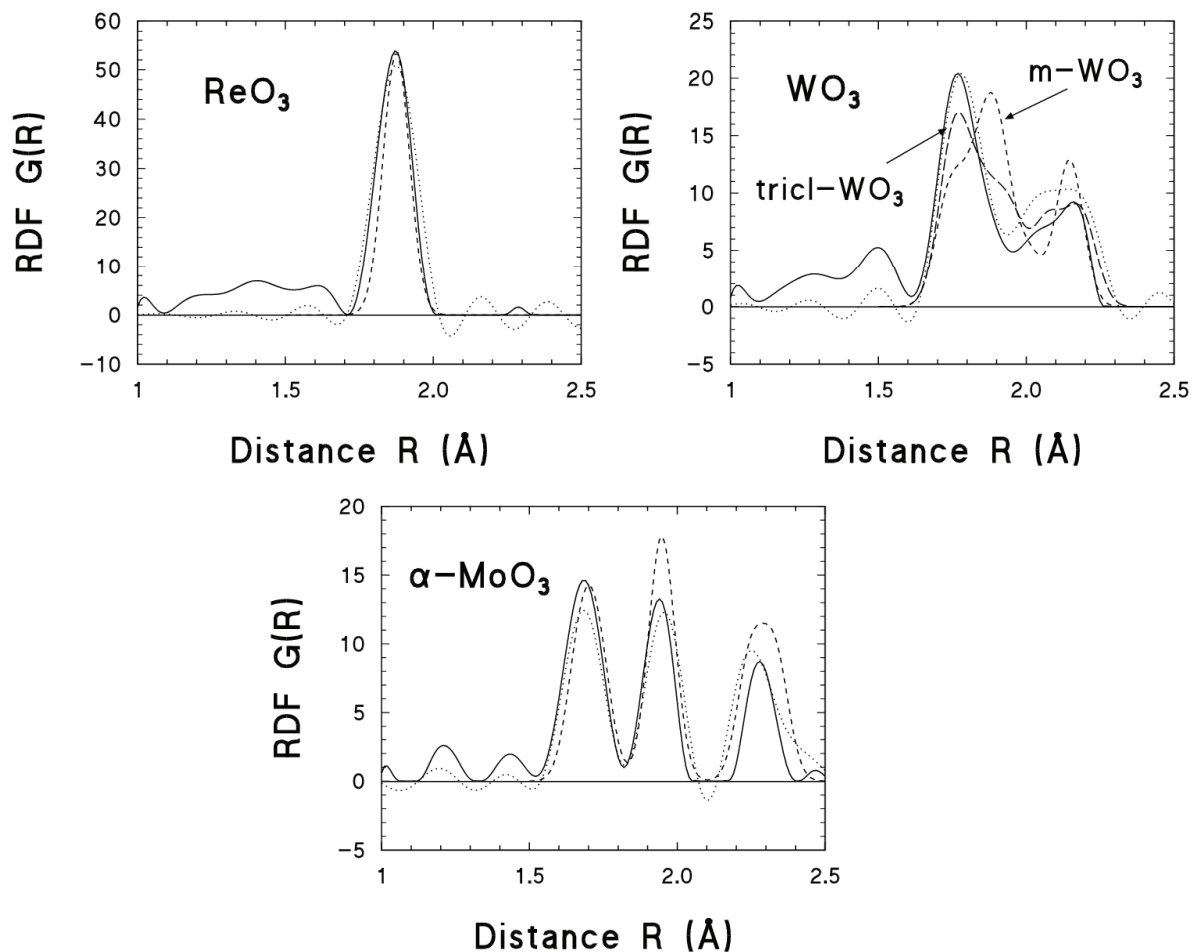
Figure 2.12: The RDFs for the first shell in ReO_3, WO_3 and α-MoO_3 derived by the splice technique (dotted lines) and by the method 3 suggested in the present work (solid lines) are compared. The positions of the interatomic distances given by the diffraction techniques [25, 26, 27] are shown by dashed lines.

2.7   Statistical analysis of the modelling results

The FTEST program allows one to perform the analysis of variances of the multi-shell fit results using the Fisher's $F_{0.95}$-test [29]. To do this, the following information is required:

- the file name for the experimental EXAFS signal used in the fit

- the file name for the first-model EXAFS signal (with smaller number of fitting parameters)

- the file name for the second-model EXAFS signal (with larger number of fitting parameters)

- the range of the fit in k-space (k_{min} and k_{max} (in Å^{-1}))

- the power n of k^n used in the analysis

- the range of the back-Fourier transform ΔR (in Å) used to single out the experimental EXAFS signal

- the number of fitting parameters M_{fit1} and M_{fit2} used in the first and second models

Using the above mentioned parameters, the program will check that the maximum number M_{max} of independent data points, allowed by the Nyquist theorem [8, 9] (see equation (2.16)), is larger than both M_{fit1} and M_{fit2} and will calculate the variances D_{fit1} and D_{fit2} according to

$$D = \frac{M_{\text{max}}}{N(M_{\text{max}} - M_{\text{fit}})} \sum_{i=1}^{N} \left(\frac{\chi_{exper}(k_i) - \chi_{model}(k_i)}{k^n} \right)^2 \tag{2.33}$$

where N is the number of points in k-space. Here it is assumed that both experimental $\chi_{exper}(k)$ and model EXAFS signals $\chi_{model}(k)$ are multiplied by the k^n factor so that a division by this factor is required for correct analysis.

According to the Fisher's $F_{0.95}$-test, the second model should be accepted when

$$\frac{D_{\text{fit1}}}{D_{\text{fit2}}} > F_{0.95} \tag{2.34}$$

where $F_{0.95}$ is the tabulated quantity [29] (the values of $F_{0.95}$ are incorporated within the FTEST code).

2.8   Visualization of the experimental and theoretical data

The EDAPLOT is a menu-based program which was designed to show simultaneously up to 20 different spectra and to carry out a set of useful operations (the option number is shown in brackets):

- input/output data files from/to disk (4 formats supported: (Y,X), (X,Y), XRD (Trento Univ.), Special for FT) (*Menu Choice 1 & 4*)

- delete spectrum from a memory (*Menu Choice 2*)

- plot spectra (several additional options are available here: change of scale, legend, axes titles and video mode, adding zero line, printer output, cursor pointer) (*Menu Choice 3*)

- EXAFS amplitude ratio and phase difference analyses (see below for details) (*Menu Choice 5,6 & 8*)

- summation, subtraction, multiplication and division of spectra (*Menu Choice 7*)

- spline and polynomial smoothing (*Menu Choice 21*)

- least-square polynomial fitting (*Menu Choice 23*)

- convolution (*Menu Choice 27*)

- spline interpolation (*Menu Choice 11*)

- calculation of the area under a curve (*Menu Choice 20*)

- calculation of the derivative (*Menu Choice 24*)

- a set of mathematical operations with X and Y axes (*Menu Choice 9,10,12,13,14 & 16*)

- corrections on the Debye-Waller factor and the core-hole broadening (*Menu Choice 17,25*)

- least-square comparison of two signals (*Menu Choice 22*)

- elimination of points (*Menu Choice 18*)

- calculation of some functions (lorenzian, gaussian, arctg, RDF, Victoreen polynomial, EXAFS signal from total amplitude and phase) (*Menu Choice 19,26 & 29*)

- calculation of shell distortion using a radial distribution function (*Menu Choice 28*)

- sorting several spectra into one by x-axis (*Menu Choice 15*)

Amplitude Ratio and Phase Difference Analyses

This method can be used to find relative variations of parameters in the EXAFS formula when the *single* shell EXAFS signal can be isolated. Such approach is commonly used for the analysis of temperature dependent EXAFS signals where the high temperature data are analysed relative to the one measured at the lowest temperature.

In the plane-wave single-scattering approximation the ratio of amplitudes and the difference of phases for two EXAFS signals $\chi(k)$ and $\chi_{et}(k)$ can be expressed as [19, 20, 21, 22]

$$\ln \frac{AMPL(k)}{AMPL_{et}(k)} = \ln \frac{NR_{et}^2}{N_{et}R^2} + \Delta C_0 - 2k^2(\sigma^2 - \sigma_{et}^2) + \frac{2}{3}k^4 \Delta C_4 \qquad (2.35)$$

$$PHASE(k) - PHASE_{et}(k) = 2k(R - R_{et}) - \frac{4}{3}k^3 \Delta C_3. \qquad (2.36)$$

In the above equations the cumulant expansion of the EXAFS function up to the 4th cumulant term is used.

2.9 Interface to the FEFF code

The EDAFEFF code allows one to extract from FEFF****.dat files, produced by the FEFF8/9 codes [5], the scattering amplitude $f(\pi, k, R)$ and phase shift $\phi(\pi, k, R)$ functions for use with EDAFIT or EDARDF codes.

2.10 Advanced methods of EXAFS data analysis

To overcome limitations of conventional EXAFS data analysis, an advanced simulation approach should be used [30, 31]. It is based on direct comparison of the experimental EXAFS spectrum with a configuration averaged EXAFS signal generated using a set of 3D atomic configurations, which can be obtained from molecular dynamics (MD) [30], Monte Carlo (MC) or reverse Monte Carlo (RMC) [31] simulations. Note that, in the first two methods, MD and MC, the knowledge of the interaction between atoms is required to take into account through the use of interatomic potentials, while no interatomic interactions are considered in the RMC technique. Such approach allows one to account simultaneously for thermal and static disorder as well as for the multiple-scattering effects. Detailed description of the advanced methods is beyond the scope of the present manual.

In the EDA package, the EDACA code allows one to perform the calculations of the configuration-averaged EXAFS based on the results of MD simulations (Fig. 2.13) [30]. To use this approach, called MD-EXAFS, one needs to provide an *.XYZ file containing temporal snapshots of atomic coordinates, which can be obtained from most MD codes such as GULP [32], DLPOLY [33] or CP2K [34] as well as the input file with a set of commands for the FEFF8/9 code.

The MD-EXAFS method was successfully applied in the past to several crystalline compounds such as ReO_3, $LaCoO_3$, NiO, ZnO, Ge and AWO_4 (A=Ca, Sr, Ba) tungstates [35].
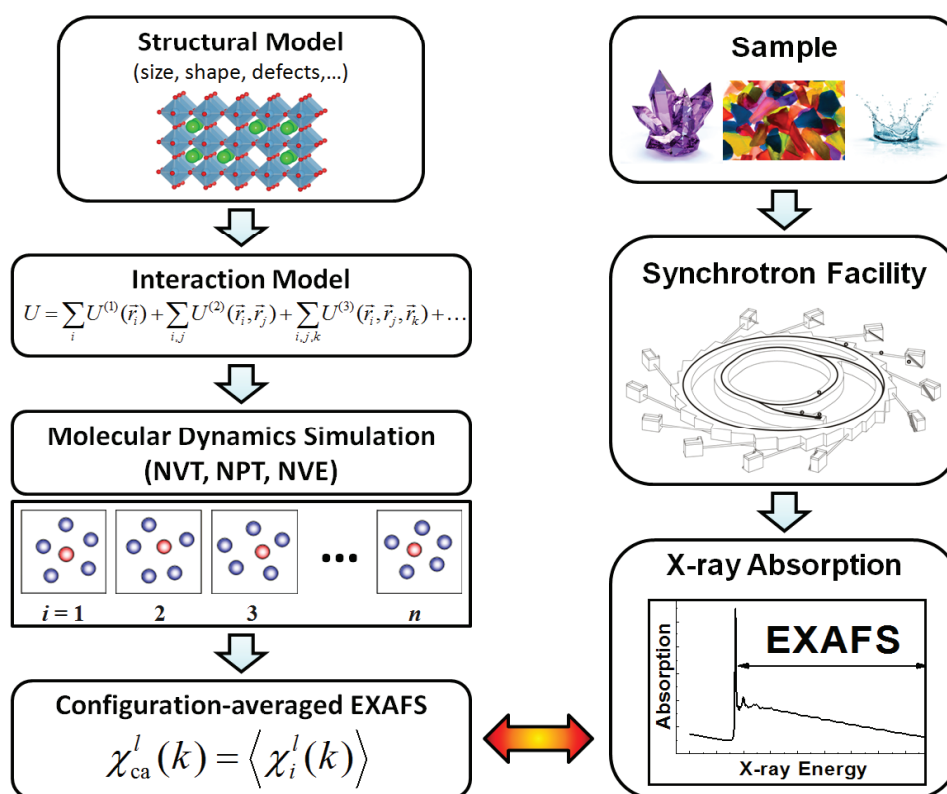
Figure 2.13: Flowchart of the MD-EXAFS calculations.

Bibliography

[1] B.K.Teo, *EXAFS: Basic Principles and Data Analysis* (Springer-Verlag, Berlin, 1986);
X-Ray Absorption: Principles, Applications, Techniques of EXAFS, SEXAFS and XANES, edited by D.C. Koningsberger and R. Prins (John Willey & Sons, New York, 1988);
V.L. Aksenov, A.Y. Kuzmin, J. Purans, and S.I. Tiutiunnikov, EXAFS spectroscopy at synchrotron-radiation beams, Phys. Part. Nucl. **32** (2001) 675-707;
A. Levina, R. S. Armstrong, P. A. Lay, Three-dimensional structure determination using multiple-scattering analysis of XAFS: applications to metalloproteins and coordination chemistry, Coord. Chem. Rev. 249 (2005) 141160;
V. L. Aksenov, M. V. Kovalchuk, A. Yu. Kuzmin, Yu. Purans, and S. I. Tyutyunnikov, Development of methods of EXAFS spectroscopy on synchrotron radiation beams, Crystallography Reports 51 (2006) 908-935 [in English]; Kristallografiya 51 (2006) 971-1000 [in Russian].

[2] A. Kuzmin, Physica B **208/209** (1995) 175-176;
A. Kuzmin, J. Physique IV (France) 7 (1997) C2-213-C2-214.

[3] A. Kuzmin and J. Purans, J. Phys.: Condens. Matter **5** (1993) 267-282;
A. Kuzmin and J. Purans, J. Phys.: Condens. Matter **5** (1993) 2333-2340;
A. Kuzmin, N. Mironova, J. Purans and A. Sazonov, Phys. Stat. Sol. (a) **135** (1993) 133-141;
G. Dalba, D. Diop, P. Fornasini, A. Kuzmin and F. Rocca, J. Phys.: Condens. Matter **5** (1993) 1643-1654;
A. Kuzmin and J. Purans, J. Phys.: Condens. Matter **5** (1993) 9423-9430;
F. Rocca, A. Kuzmin, J. Purans and G. Mariotto, Solid State Ionics **70/71** (1994) 465-470;
A. Kuzmin, N. Mironova, J. Purans and A. Rodionov, J. Phys.: Condensed Matter **7** (1995) 9357-9368;
F. Rocca, A. Kuzmin, J. Purans and G. Mariotto, Phys. Rev. B **53** (1996) 11447-

11450;

A. Kuzmin, J. Purans, G. Dalba, P. Fornasini and F. Rocca, J. Phys.: Condens. Matter **8** (1996) 9083-9102. J. Purans, A. Kuzmin and C. Guéry, in *Optical Organic and Semiconductor Inorganic Materials*, eds. E.A. Silinsh, A. Medvid, A.R. Lusis and A.O. Ozols, SPIE Proc. **2968** (1997) 174-179;

A. Kuzmin and J. Purans, in *Optical Organic and Semiconductor Inorganic Materials*, eds. E.A. Silinsh, A. Medvid, A.R. Lusis, A.O. Ozols, SPIE Proc. **2968** (1997) 180-185;

A. Kuzmin, N. Mironova and J. Purans, J. Phys.: Condensed Matter **9** (1997) 5277-5286;

A. Kuzmin, J. Purans and A. Rodionov, J. Phys.: Condensed Matter **9** (1997) 6979-6993;

A. Kuzmin, S. Obst and J. Purans, J. Phys.: Condensed Matter **9** (1997) 10065-10078;

F. Rocca, G. Dalba, R. Grisenti, M. Bettinelli, F. Monti and A. Kuzmin, J. Non-Cryst. Solids **232-234** (1998) 581-586;

A. Kuzmin, J. Purans, E. Cazzanelli, C. Vinegoni and G. Mariotto, J. Appl. Phys. **84** (1998) 5515-5524;

F. Rocca, A. Dalmasso, F. Monti, A. Kuzmin and D. Pasqualini, J. Synchrotron Rad. **6** (1999) 737-739;

F. Rocca, A. Kuzmin, P. Mustarelli, C. Tomasi, and A. Magistris, Solid State Ionics **121** (1999) 189-192;

A. Kuzmin and J. Purans, J. Phys.: Condensed Matter **12** (2000) 1959-1970;

A. Kuzmin, J. Purans and A. Sternberg, in "Defects and Surface-Induced Effects in Advanced Perovskites", edited by G. Borstel, A. Krumins, and D. Millers, NATO ASHT, Ser. 3, Vol. 77, (Kluwer, Dordrecht, 2000), 145-150;

A. Kuzmin, J. Purans, R. Kalendarev, D. Pailharey and Y. Mathey, Electrochim. Acta **46** (2001) 2233-2236;

F. Rocca, M. Ferrari, A. Kuzmin, N. Daldosso, C. Duverger, and F. Monti, J. Non-Cryst. Solids **293-295** 2001) 112-117;

A. Kuzmin and J. Purans, crystals, Rad. Measurements **33** (2001) 583-586;

F. Rocca, C. Armellini, M. Ferrari, G. Dalba, N. Diab, A. Kuzmin, and F. Monti, J. Sol-Gel Sci. Tech. **26** (2003) 267-271;

J. Gaidelene, R. Kalendarev, A. Kuzmin, and J. Purans, Nucl. Instrum. Methods Phys. Res. A **531** (2004) 321-326;

A. Kuzmin, G. Dalba, P. Fornasini, F. Rocca, and O. Sipr, Phys. Rev. B **73** (2006) 174110:1-12;

M. Vračar, A. Kuzmin, R. Merkle, J. Purans, E. A. Kotomin, J. Maier, and O. Mathon, Phys. Rev. B **76** (2007) 174107:1-12;

J. Purans, N.D. Afify, G. Dalba, R. Grisenti, S. De Panfilis, A. Kuzmin, V.I. Ozhogin, F. Rocca, A. Sanson, S.I. Tiutiunnikov, and P. Fornasini, Phys. Rev. Lett. **100** (2008) 055901:1-4;

A. Anspoks, A. Kuzmin, A. Kalinko, and J. Timoshenko, Solid State Commun. **150** (2010) 2270-2274;

A. Kalinko and A. Kuzmin, J. Non-Cryst. Solids **357** (2011) 2595-2599.

[4] J.J. Rehr, J. Mustre de Leon, S.I. Zabinsky, and R.C. Albers, J. Am. Chem. Soc. **113** (1991) 5135-5140;
J. Mustre de Leon, J.J. Rehr, S.I. Zabinsky, and R.C. Albers, Phys. Rev. B **44** (1991) 4146-4156.

[5] A. L. Ankudinov, B. Ravel, J. J. Rehr, S. D. Conradson, Phys. Rev. B **58** (1998) 7565.

[6] M.F. Ruiz-López, F. Bohr, A. Filipponi, A. Di Cicco, T.A. Tyson, M. Benfatto and C.R. Natoli, in *Proc. 6th Inter. Conf. on X-ray Absorption Fine Structure, York*, edited by S.S. Hasnain (Ellis Horwood, Singapore, 1991) p.75;
T.A. Tyson, *Ph.D. Thesis*, Stanford University, 1991.

[7] J.P. Lee and M.B. Comisarow, Appl. Spectrosc. **43** (1989) 599-604.

[8] E.O. Brigham, *The Fast Fourier Transform* (Prentice Hall, Englewood Cliffs, New Jersey, 1974).

[9] E.A. Stern, Phys. Rev. B **48** (1993) 9825.

[10] J. Purans, A. Kuzmin, Ph. Parent and H. Dexpert, Physica B **208/209** (1995) 373-374.

[11] J. Purans, A. Kuzmin, Ph. Parent and H. Dexpert, Physica B **208/209** (1995) 307-308.

[12] A. Filipponi, A. Di Cicco, M. Benfatto and C.R. Natoli, Europhys. Lett. **13** (1990) 319.

[13] L. Hedin and B.I. Lundqvist, J. Phys.: Solid State Phys. **4** (1971) 2064.

[14] Yu.A. Babanov, V.V. Vasin, A.L. Ageev and N.V. Ershov, Phys. Status Solidi (b) **105** (1981) 747-754;

N.V. Ershov, A.L. Ageev, V.V. Vasin and Yu.A. Babanov, Phys. Status Solidi (b) **108** (1981) 103-111.

[15] A.N. Tikhonov and V.Ya. Arsenin, *Metody resheniya nekorrektnykh zadach* (Izd. Nauka, Moskva, 1979);
A. Bakushinsky and A. Goncharsky, *Ill-Posed Problems: Theory and Applications* (Kluwer Academic Publishers, Dordrecht, 1994).

[16] C. Lanczos, *Applied Analysis* (Prentice Hall, 1956).

[17] E.A. Stern, Y. Ma, O. Hanske-Petitpierre and C.E. Bouldin, Phys. Rev. B **46** (1992) 687-694.

[18] C.E. Bouldin and E.A. Stern, in *EXAFS and Near Edge Structure III* edited by K.O. Hodgson, B. Hedman and J.E. Penner-Hahn (Springer, Berlin, 1984) pp. 273-277.

[19] G. Bunker, Nucl. Instrum. & Methods A **207** (1983) 437-444.

[20] J.M. Tranquada and R. Ingalls, Phys. Rev. B **28** (1983) 3520-3528.

[21] E.D. Crozier, J.J. Rehr and R. Ingalls in *X-Ray Absorption: Principles, Applications, Techniques of EXAFS, SEXAFS and XANES* edited by D. C. Koningsberger and R. Prins (Wiley, New York, 1988) p. 373.

[22] G. Dalba, P. Fornasini and F. Rocca, Phys. Rev. B **47** (1993) 8502-8514.

[23] A. Filipponi, J. Phys.: Condens. Matter **6** (1994) 8415-8427.

[24] A. Filipponi and A. Di Cicco, Phys. Rev. B **51** (1995) 12322-12336.

[25] J.E. Jørgensen, J.D. Jorgensen, B. Batlogg, J.P. Remeika and J.D. Axe, Phys. Rev. B **33** (1986) 4793-4798.

[26] B.O. Loopstra and H.M. Rietveld, Acta Cryst. B **25** (1969) 1420.

[27] S. Crouch-Baker and P.G. Dickens, Solid State Ionics **32/33** (1989) 219.

[28] J.J. Rehr, C.H. Booth, F. Bridges and S.I. Zabinsky, Phys. Rev. B **49** (1994) 12347-12350.

[29] E.I. Pustyl'nik, *Statisticheskie metody analiza i obrabotki nabludenii* (Izd. Nauka, Moskva, 1968);
D.J. Hudson, *Statistics: Lectures on Elementary Statistics and Probability* (CERN, Geneva, 1964).

[30] A. Kuzmin and R.A. Evarestov, J. Phys.: Condens. Matter **21** (2009) 055401 (6 pp);
A. Kuzmin and R.A. Evarestov, J. Phys.: Conf. Series **190** (2009) 012024 (6pp);
A. Kuzmin and J. Chaboy, IUCrJ **1** (2014) 571-589;
A. Kuzmin, A. Anspoks, A. Kalinko, J. Timoshenko, Z. Phys. Chem. **230** (2016) 537-549.

[31] J. Timoshenko, A. Kuzmin, J. Purans, J. Phys.: Condens. Matter **26** (2014) 055401 (15pp);
J. Timoshenko, A. Kuzmin, and J. Purans, Comp. Phys. Commun. **183** (2012) 1237-1245;
J. Timoshenko, A. Anspoks, A. Kalinko, A. Kuzmin, Z. Phys. Chem. **230** (2016) 551-568.

[32] J. D. Gale and A. L. Rohl, Mol. Simul. **29** (2003) 291341.

[33] I. T. Todorov, W. Smith, K. Trachenko, M. T. Dove, J. Mater. Chem. **16** (2006) 19111918.

[34] J. VandeVondele, M. Krack, F. Mohamed, M. Parrinello, T. Chassaing, J. Hutter, Comp. Phys. Commun. **167** (2005) 103128.

[35] A. Kalinko, R.A. Evarestov, A. Kuzmin, and J. Purans, J. Phys.: Conf. Series **190** (2009) 012080 (4pp);
A. Anspoks and A. Kuzmin, J. Non-Cryst. Solids **357** (2011) 2604-2610;
A. Anspoks, A. Kuzmin, A. Kalinko, and J. Timoshenko, Solid State Commun. **150** (2010) 2270-2274;
A. Kuzmin, V. Efimov, E. Efimova, V. Sikolenko, S. Pascarelli, I. O. Troyanchuk, Solid State Ionics **188** (2011) 21-24;
J. Timoshenko, A. Kuzmin, and J. Purans, Centr. Eur. J. Phys. **9** (2011) 710-715;
J. Timoshenko, A. Anspoks, A. Kalinko, A. Kuzmin, Acta Mater. **79** (2014) 194-202.